Genomically Complex Human Angiosarcoma and Canine Hemangiosarcoma Establish Convergent Angiogenic Transcriptional Programs

Jong Hyuk Kim[1,2,3,4*], Kate Megquier[5], Rachael Thomas[6], Aaron L. Sarver[1,3,7], Jung Min Song[3], Yoon Tae Kim[8], Nuojin Cheng[9], Ashley J. Schulte[1,2,3], Michael A. Linden[1,3,10], Paari Murugan[1,3,10], LeAnn Oseth[3], Colleen L. Forster[11], Ingegerd Elvers[5,12], Ross Swofford[5], Jason Turner-Maier[5], Elinor K. Karlsson[5,13], Matthew Breen[6,14], Kerstin Lindblad-Toh[5,12], Jaime F. Modiano[1,2,3,4,10,15,16]

[1]Animal Cancer Care and Research Program, University of Minnesota, St Paul, MN, USA

[2]Department of Veterinary Clinical Sciences, College of Veterinary Medicine, University of Minnesota, St Paul, MN, USA

[3]Masonic Cancer Center, University of Minnesota, Minneapolis, MN, USA

[4]Institute for Engineering in Medicine, University of Minnesota, Minneapolis, MN, USA

[5]Broad Institute of Harvard and MIT, Cambridge, MA, USA

[6]Department of Molecular Biomedical Sciences, College of Veterinary Medicine & Comparative Medicine Institute, North Carolina State University, Raleigh, NC, USA

[7]Institute for Health Informatics, University of Minnesota, Minneapolis, MN, USA

[8]Department of Electrical Engineering and Computer Science, York University, Toronto, Ontario, Canada

[9]School of Mathematics, College of Science and Engineering, University of Minnesota, Minneapolis, MN, USA

[10]Department of Laboratory Medicine and Pathology, School of Medicine, University of Minnesota, Minneapolis, MN, USA

[11]The University of Minnesota Biological Materials Procurement Network (BioNet), University of Minnesota, Minneapolis, MN, USA

[12]Science for Life Laboratory, Department of Medical Biochemistry and Microbiology, Uppsala University, Uppsala, Sweden

[13]University of Massachusetts Medical School, Worcester, MA, USA

[14]Cancer Genetics Program, University of North Carolina Lineberger Comprehensive Cancer Center, Raleigh, NC, USA

[15]Center for Immunology, University of Minnesota, Minneapolis, MN, USA

[16]Stem Cell Institute, University of Minnesota, Minneapolis, MN, USA

*Corresponding author: Jong Hyuk Kim (jhkim@umn.edu), Masonic Cancer Center, University of Minnesota, Minneapolis, MN 55455

One Sentence Summary: This study shows that, while drive events of malignant vasoformative tumors of humans and dogs include diverse mutations and stochastic rearrangements that create novel fusion genes, convergent transcriptional programs govern the highly conserved morphological organization and biological behavior of these tumors in both species.

Abstract

Sporadic angiosarcomas (ASs) are aggressive vascular sarcomas whose rarity and genomic complexity present significant obstacles in deciphering the pathogenic significance of individual genetic alterations. Numerous fusion genes have been identified across multiple types of cancers, but their existence and significance remain unclear in sporadic ASs. In this study, we leveraged RNA sequencing data from thirteen human ASs and 76 spontaneous canine hemangiosarcomas (HSAs) to identify fusion genes associated with spontaneous vascular malignancies. Ten novel protein-coding fusion genes, including *TEX2-PECAM1* and *ATP8A2-FLT1*, were identified in seven of the thirteen human tumors, with two tumors showing mutations of *TP53*. *HRAS* and *NRAS* mutations were found in ASs without fusions or *TP53* mutations. We found fifteen novel protein-coding fusion genes including *MYO16-PTK2*, *GABRA3-FLT1*, and *AKT3-XPNPEP1* in eleven of the 76 canine HSAs; these fusion genes were seen exclusively in tumors of the angiogenic molecular subtype that contained recurrent mutations in *TP53*, *PIK3CA*, *PIK3R1*, and *NRAS*. In particular, fusion genes and mutations of *TP53* co-occurred in tumors with higher frequency than expected by random chance, and they enriched gene signatures predicting activation of angiogenic pathways. Comparative transcriptomic analysis of human ASs and canine HSAs identified shared molecular signatures associated with activation of PI3K/AKT/mTOR pathways. Our data suggest that genomic instability induced by *TP53* mutations might create a predisposition for fusion events that may contribute to tumor progression by promoting selection and/or enhancing fitness through activation of convergent angiogenic pathways in this vascular malignancy.

Keywords: Angiosarcoma, chromosome translocation, fusion gene, hemangiosarcoma, *TP53*

24 **Introduction**

25 Sarcomas are diverse tumors that arise from cells of mesenchymal origin in soft tissues
26 such as blood and lymphatic vessels, fat, bone, cartilage, muscle, and connective tissues. The
27 heterogeneity of sarcomas has provided an impetus for developing molecular approaches to
28 classify these tumors (*1, 2*), leading to their categorization into genomically simple and
29 genomically complex sarcomas (*1, 3*). Angiosarcomas (ASs) are rare, highly aggressive,
30 genomically complex sarcomas of blood vessel-forming cells (*3, 4*). The five-year survival rate
31 of AS is approximately 40% (*5-7*), but half of patients have metastatic or unresectable disease
32 with a median overall survival of less than 6 months (*8*). The events that drive progression are
33 incompletely understood; previous studies have identified recurrent mutations of *RAS*, *PTPRB*,
34 *PLCG1*, *KDR* (kinase insert domain receptor, also known as *VEGFR2*), *TP53*, *PIK3CA*, and
35 *FLT4* (*VEGFR3*) in human ASs (*9-12*). *MYC* gene amplification and alterations in the TP53,
36 CDKN2, NF-κB/IL-6, PIK3CA/AKT/mTOR pathways have also been reported (*13*); however,
37 these studies represent a small case series, precluding definitive conclusions regarding
38 pathogenic mechanisms that contribute to the genetic cause and to the progression of the disease.

39 Hemangiosarcoma (HSA) is a malignant vascular tumor that is common in dogs with an
40 estimated tens of thousands of cases diagnosed each year (*14-16*). Canine HSA shares clinical
41 and morphological features with human AS, as well as aspects of its mutational landscape (*17-*
42 *20*). We previously documented three molecular subtypes of HSA, characterized by angiogenic,
43 inflammatory, and adipogenic transcriptomic signatures (*21*). These gene expression signatures
44 are conserved in HSA progenitor cells that show multipotency and self-renewal (*21*).
45 Nevertheless, the transcriptional state of these HSA progenitor cells seems to be somewhat
46 malleable, regulated by immune and metabolic reprogramming (*22*). Mutations in genes that

47 regulate genomic integrity, such as *TP53,* can alter the intrinsic transcriptional program of tumor
48 cells; however, genomic instability in the tumor can create even more dramatic changes by
49 modulating transcriptional programs of heterotypic stromal cells in the tumor tissue, as well as in
50 the composition of the niche (*23, 24*).

51 Chromosome translocations and the resulting fusion genes are important contributors to
52 the pathogenesis of cancer, particularly in sarcomas and hematopoietic malignancies (*25*).
53 However, the nature and frequency of these events in canine HSA and human AS remains
54 unclear. Here, we used next generation RNA sequencing (RNA-Seq) data to identify fusion
55 genes in thirteen human ASs and 76 visceral HSAs originating from 74 dogs, and we
56 investigated the relationship of these fusions to the mutational landscape of the tumor. We
57 identified ten novel protein-coding fusion genes including *TEX2-PECAM1* and *ATP8A2-FLT1* in
58 seven of thirteen human ASs, and two of the fusion-detected tumors showed mutations of *TP53*
59 (R248Q and P250L). In canine HSAs, we found novel protein-coding fusion genes in a subset of
60 the tumors of the angiogenic subtype. These fusion genes co-occurred with *TP53* mutations and
61 were associated with gene enrichment for activated angiogenic pathways in the tumors. Our data
62 suggest that genomic instability induced by mutations of *TP53* creates a permissive environment
63 for fusion genes, with selection for angiogenic molecular programs in malignant vasoformative
64 tumors. Our data also demonstrate that human AS and canine HSA maintain molecular programs
65 that activate convergent signaling pathways to establish angiogenic phenotypes despite their
66 genomic complexity.

67

68 **Results**

69

70 **Novel protein-coding fusion genes are identified in human ASs and canine HSAs**

71 Putative fusion gene events were identified from RNA-Seq data as paired-end sequence reads
72 that mapped connecting two distant genes (**fig. S1A**). We identified novel in-frame protein-
73 coding fusion transcripts for ten fusion events in 7 of 13 (53.8%) human ASs **(Fig. 1A** and **Table**
74 **1)**. Two of the fusions were inter-chromosomal events and eight were intra-chromosomal events.
75 The fusions included *TEX2-PECAM1*, which contained the gene that encodes CD31, and
76 *ATP8A2-FLT1*, a kinase fusion gene that encodes the vascular endothelial growth factor receptor
77 1 (VEGFR1). None of the ten fusion events was seen in more than one tumor, and three of the
78 seven fusion-positive tumors contained two distinct fusion events each.

79 In canine HSA, we found fifteen novel protein-coding fusion genes in eleven of 76
80 tumors (14.5%) (**Table 2** and **Fig. 1B**). Ten of the fusions were inter-chromosomal events and
81 five were intra-chromosomal events. None of the fifteen fusion events was seen in more than one
82 tumor, and four of the eleven fusion-positive tumors involved two distinct fusion genes each.
83 One fusion partner in four of the translocations encoded either a protein kinase or a protein
84 phosphatase associated with angiogenic signaling (*MYO16-PTK2, GABRA3-FLT1*, *AKT3-*
85 *XPNPEP1,* and *PTPRB-NOL10*). Eight of the fusion genes were associated with kinase signaling
86 or kinase binding activity, such as PI3 kinase signaling, a MAP kinase, a receptor tyrosine
87 kinase, a protein serine/threonine kinase, and an NAD+ kinase. Gene ontology annotations of the
88 fusion partners for every translocation are described in **table S4** for human AS and **table S5** for
89 canine HSA. Fusion genes were not present in any of the human non-malignant tissues ($N = 6$) or
90 canine hematomas ($N = 10$) examined. Conserved driver translocations such as *BCR-ABL* and
91 *MYC-IGH* that are present in both human and canine chronic myelogenous leukemia and Burkitt
92 lymphoma, respectively (*26*), were not identified in human AS and canine HSA. That is, all the

93 fusion events identified in the seven human ASs and eleven canine HSAs involved different gene
94 pairs, with the exception of the *FLT1* gene, which created fusions with a different partner gene in
95 one case from each species.

96 To determine whether the non-tumor components in the tumor tissue affected the
97 detection of fusion genes, we quantified tumor content histologically and bioinformatically in
98 canine HSAs **(fig. S2A-E**). Seventy of the 76 HSA samples were histologically evaluated, and
99 the tumor content was not different between HSA samples with fusion events ($N = 11$) and those
100 without fusion events ($N = 59$). We used two independent bioinformatic tools, *xCell* and
101 ESTIMATE, to predict stromal and immune cell components, and these algorithms generated
102 consistent output scores (Pearson's $R = 0.84$; $R^2 = 0.71$; $P < 0.00001$) that showed the presence of
103 fusion genes was not associated with tumor purity. The detection of fusion genes was also
104 independent of sequencing depth (**fig. S2F**). To rule out artifacts from the computational process,
105 we validated four representative fusion transcripts found in canine HSAs (*MYO16-PTK2*; *AKT3-*
106 *XPNPEP1*; *AP4E1-BAIAP2*; *NOL10-PTPRB*) by RT-PCR. PCR primer pairs were designed to
107 amplify putative split sequences (up to 200 base pairs) involving the breakpoints identified by
108 deFuse (**fig. S3A**). We confirmed that the junction sequences between the two genes producing
109 the new fusion event were amplified by PCR in each case (**fig. S3B-C**), with each PCR
110 amplification product verified by Sanger sequencing. We then used RT-PCR to evaluate RNA-
111 Seq data from 63 canine tissue samples (53 HSAs and 10 hematomas) for the presence of the
112 four fusion transcripts. The results were consistent between RNA-Seq and PCR, as we found
113 neither false-positive nor false-negative events in the samples tested (**table S6**).
114

115 **Fusion genes are associated with DNA copy number variations**

116 We then determined if any of the fusion partner genes identified in our analysis were associated
117 with DNA copy number alterations. Publicly available whole Exome-sequencing data generated
118 from an independent data set of 36 human patients with ASs was used (*12*). Copy number
119 variations were found in twelve of the twenty (60%) fusion partner genes: nine genes were
120 amplified, and five genes were deleted (**Fig. 1C** and **fig. S4)**. *TEX2* (39%), *STEAP1B* (25%) and
121 *PECAM1* (25%) were the top three genes where copy number gains occurred most frequently.
122 For canine HSA, we used oligonucleotide array comparative genomic hybridization (oaCGH) in
123 a larger HSA dataset (*N* = 123) (*19*). Copy number gains were observed in 29 of the 30 (96.7%)
124 fusion partners, and copy number losses were observed in 27 of the 30 (90.0%) fusion partners.
125 Protein kinase-encoding genes, *PTK2*, *FLT1*, and *AKT*3 revealed a higher frequency of copy
126 number gain: 15.5% gain vs 0.8% loss for *PTK2*; 4.9% gain vs 0.8% loss for *FLT1*; and 4.1%
127 gain vs 0.8% loss for *AKT3*, suggesting that copy number alterations leading to dysregulation of
128 downstream kinase signaling contribute at least partly to the angiogenic program in a subset of
129 canine HSAs (**Fig. 1D**).
130

131 **Chromosomal translocations resulting in fusion genes are detectable in canine HSAs**

132 We performed fluorescence *in situ* hybridization (FISH) to confirm that fusion genes were
133 generated by chromosome translocations. We chose representative inter-chromosomal fusions,
134 *MYO16-PTK2* and *GABRA3-FLT1* for cytogenetic validation because PTK2 and VEGFR1 are
135 key molecules that regulate pathogenic signaling in vascular cancers, including canine HSA (*27*).
136 **Fig. 2A** illustrates the predicted structure of *MYO16-PTK2* inter-chromosomal fusion between
137 CFA 22 and CFA 13, based on deFuse and Sanger sequencing data (**Fig. 2B**). The predicted
138 fusion gene comprises exons 1-32 of *MYO16* (CFA 22) and exons 12-31 of *PTK2* (CFA 13),

139 with the putative junction joining *MYO16* exon 32 and *PTK2* exon 12. Breakage occurs between
140 exons 32 and 33 of *MYO16* at CFA 22:57,750,807 bp, and between exons 11 and 12 of *PTK2* at
141 CFA 13:35,397,284 bp. Independent FISH probes identifying the association between proximal
142 and distal *MYO16* and the breakpoint of *PTK2* (**Fig. 2C**) confirmed the presence of the *MYO16-*
143 *PTK2* fusion gene between CFA 22 and 13 in archival formalin fixed paraffin embedded (FFPE)
144 samples from the same dog tumor. The *MYO16-PTK2* fusion was identified by deFuse and RT-
145 PCR (**Fig. 2D**). The t(CFA 13;CFA 22) translocation was present in interphase nuclei of 16.8%
146 of the tumor cells, with a smaller subpopulation showing amplification of the fusion (**Fig. 2E**).
147 We used break-apart FISH to validate the presence of the *GABRA3-FLT1* fusion gene
148 (**Fig. 2F**). Split *FLT1* probes were found in 36.7% of tumor cells in archival FFPE samples from
149 the dog tumor in which the *GABRA3-FLT1* fusion was identified by deFuse and RT-PCR.
150 Interestingly, in this tumor the intact *FLT1* gene showed consistent amplification (up to four
151 copies), suggesting Flt-1 (also known as VEGFR1) activation in this tumor might have occurred
152 through multiple mechanisms (**Fig. 2G**). We next used FISH analysis to assess recurrence of the
153 *MYO16-PTK2* fusion in a tissue microarray (TMA) comprised of 45 visceral HSAs and eight
154 non-malignant tissues (six spleens; two livers). The *MYO16-PTK2* fusion was once again present
155 in the sample from the canine tumor in which it was discovered, but it was not seen in any other
156 sample on the TMA. We also performed FISH to detect the *ATP8A2-FLT1* fusion in human AS
157 using a break-apart *FLT1* probe, but the fusion was undetectable in our FFPE sample. This might
158 have been due to the small number of tumor cells that were likely to contain the fusion event in a
159 heterogeneous clonal population. Since none of the fusion transcripts identified in our cohorts of
160 human and canine tumors were recurrent, we sought to determine if the fusion events were
161 associated with other genetic and molecular programs.

162

163 **Fusion genes and somatic variants in human ASs enrich angiogenic gene signatures**

164 To examine genomic aberrations associated with the fusion genes, we determined somatic
165 variations and gene expression profiles using RNA-Seq data. In human ASs, *TP53* mutations
166 (R248Q and P250L) were observed in two of thirteen human ASs, which also had fusion genes
167 (*SMURF1-TMEM139* and *AGO2-TRAPPC9* in one tumor, *IRF9-THTPA* in the other tumor).
168 *NRAS* (Q61L; $N = 1$) or *HRAS* (Q61L; $N = 1$) mutations were also detected, and both were
169 present in tumors that did not have fusion genes or *TP53* mutations (**Fig. 3A** and **Table 1**). The
170 RNA-Seq data did not provide evidence of mutations in *PIK3CA, PTEN*, or *KRAS* in this group
171 of thirteen ASs.

172 We established transcriptomic profiles of human ASs to identify molecular traits that
173 regulate global gene expression. We identified 1,237 differentially expressed genes between ASs
174 ($N = 13$) and non-malignant controls ($N = 6$) (FDR P-value < 0.05): 490 genes were upregulated
175 and 747 genes were downregulated in ASs. Biological functions and pathway analysis revealed
176 that upregulated genes in ASs were associated with cancer, angiogenesis, vasculogenesis, and
177 development of vasculature ($P < 0.00001$) (**table S7**). Additionally, we performed cell type
178 enrichment analysis using the *xCell* tool (*28*) to predict relative populations of cellular
179 components that comprised the AS tissues (**fig. S5**). We compared the cell type signature of AS
180 with that of sarcomas ($N = 263$) from The Cancer Genome Atlas (TCGA) database, which did
181 not include AS. The results showed that gene signatures associated with endothelial cells and
182 activated dendritic cells were highly enriched in ASs, while other sarcomas in the TCGA
183 revealed gene enrichment of smooth muscle cells. Gene expression profiles of non-malignant
184 samples indicated distinct tissue-specific patterns of submandibular gland, skin, breast adipose

185 tissue, thigh skeletal muscle, spleen, and lung. The ASs showed upregulation of key angiogenic
186 genes such as *PECAM1* (*CD31*), *FLT1* (*VEGFR1*), *KDR* (*VEGFR2)*, and *FLT4* (*VEGFR3)*
187 compared to non-malignant tissues (**Fig. 3B**). In addition, 6 of 20 (30.0%) fusion partners
188 (including *PECAM1*) showed a higher level of expression in the tumors compared to non-
189 malignant tissues ($P < 0.05$; fold change in a range from 1.9 to 35.0) (**Fig. 3C**). Collectively, our
190 data showed enriched angiogenic molecular programs were present in human ASs. Furthermore,
191 both tumors with *TP53* mutations also harbored fusion genes.
192
193 **Fusion genes that co-occur with mutations of *TP53* are present exclusively in angiogenic**
194 **canine HSAs**
195 In canine HSAs, *TP53* (N = 24/74; 32.4%), *PIK3CA* (N = 16/74; 21.6%), *PIK3R1* (N = 5/74;
196 6.8%), and *NRAS* (N = 4/74; 5.4%) transcripts showed recurrent mutations that were consistent
197 with those identified using tumor:normal Exome-sequencing (*17*). We found associations
198 between mutations of *TP53* (*TP53*^{mt}) and *PIK3CA* (*PIK3CA*^{mt}) and fusion genes (Fusion^{+}) (**table**
199 **S8**). Specifically, *TP53*^{mt} commonly co-occurred with *PIK3CA*^{mt} (P = 0.004) and with fusion
200 genes (P = 0.004); and Fusion^{+} tumors were seen in the tumors with *TP53*^{mt} or *PIK3CA*^{mt} (P =
201 0.005) more frequently than would be expected by random chance. When fusion genes co-
202 occurred with *PIK3CA*^{mt}, they invariably co-occurred with mutations of *TP53* (P = 0.037), and
203 they were not associated with *PIK3CA*^{mt} alone (P = 0.324).
204 Next, we sought to determine if fusion genes were preferentially associated with specific
205 molecular subtypes of canine HSA. We previously defined distinct angiogenic, inflammatory,
206 and adipogenic molecular subtypes of canine HSA (*21*). To further validate this classification,
207 we applied unsupervised principal component analysis (PCA) and hierarchical clustering to

208 identify distinct groups in the sample cohort from this study (**fig. S6**). Our results show that the
209 three molecular subtypes (58 angiogenic, 14 inflammatory, and 4 adipogenic) were reproducibly
210 identified in the current dataset, as illustrated in the heatmap of 1,477 differently expressed genes
211 (DEGs) (FDR $P < 0.001$; fold change > |3|) shown in **Fig. 3D**. Interestingly, fusion genes were
212 present only in tumors of the angiogenic HSA subtype ($P = 0.046$). Likewise, *TP53* mutations
213 were identified in 23 of 56 (41.1%) angiogenic HSAs, and in one of 18 tumors from the two
214 other molecular subtypes ($P = 0.008$). The somatic variants of *TP53*, *PIK3CA*, *PIK3R1*, and
215 *NRAS* were found in 33 of 56 (58.9%) angiogenic HSAs, and in 3 of 18 (16.7%) tumors from the
216 two other subtypes ($P = 0.002$). The angiogenic subtype of HSA also showed upregulation of
217 *PECAM1* (*CD31*), *FLT1* (*VEGFR1*), *KDR* (*VEGFR2)*, and *FLT4* (*VEGFR3)* compared to the
218 other two HSA subtypes and to non-malignant hematomas (**Fig. 3E**). We found that five of 32
219 dogs (16%) with angiogenic HSA lived longer than five months, while four of 10 dogs (40%)
220 with inflammatory HSA survived longer than that (**fig. S7**). Eighteen of 30 (60.0%) fusion
221 partners, including protein kinase-encoding genes such as *FLT1*, *PTK2*, and *AKT3,* showed
222 higher levels of expression in HSAs compared to non-malignant controls ($P < 0.05$; fold change
223 in a range from 1.3 to 6.0) (**Fig. 3F**). Neither breed, sex, neuter status, age, nor affected organs
224 were associated with the presence of fusion genes (**fig. S8**). There was also no association
225 between the fusion events and histological subtype or mitotic index (**table S9**).
226 Next, we analyzed DEGs (FDR $P < 0.05$; fold change > |2|) and gene pathways to
227 examine gene signatures enriched in HSAs that had both fusion genes and *TP53* mutations. We
228 classified tumors according to their mutations as summarized in **table S10**. Co-occurrence of
229 fusion genes with *TP53* mutations (i.e., $TP53^{mt}$/$Fusion^{+}$/$PIK3CA^{wt}$ or PF tumors) was associated
230 with angiogenic and vascular signaling with enrichment of genes in pathways such as PI3K,

231 VEGF, and PDGF (**tables S11-S13**). Thirteen genes that were commonly enriched in PF tumors
232 were associated with activation of WNT3A as an upstream regulator (**fig. S9**). **Fig. 4** illustrates a
233 model integrating the data from these findings to highlight potential pathogenetic contributions
234 of fusion genes and recurrent mutations in canine HSA.
235

236 **Human ASs and canine HSAs establish molecular programs that activate convergent**
237 **signaling pathways**

238 To determine if the genetic and molecular features of human AS and canine HSAs contributed to
239 the activation of functional pathways, we performed immunohistochemistry (IHC) in eleven
240 human AS tissues and in 44 canine HSAs (**Fig. 5; tables S14 - S15**). First, we evaluated the
241 effects of *TP53* mutation on the presence and location of p53, phospho-p53 (Ser15), and
242 phospho-p53 (Ser20) (**Fig. 5A-B)**. In human ASs, nuclear expression of p53 was found in all of
243 eleven (100%) tumors, showing various levels of expression. Nuclear expression of phospho-p53
244 (Ser15) was seen in seven of eleven (63.6%) tumors, showing low expression in five of seven
245 (71%) tumors (IHC score ≤ 3). Nuclear and cytoplasmic expression of phospho-p53 (Ser20)
246 protein was detected in all eleven (100%) tumors, and seven of those showed high expression
247 (IHC score ≥ 7). In canine HSAs, p53 protein was localized to the nucleus in 34 of 44 (77%)
248 tumors with various levels of expression. Immunoreactivity of phospho-p53 (Ser15) was
249 observed in the nuclei of tumor cells in 38 of 40 (95%) cases, with 34 (90%) showing low or
250 medium expression (IHC score ≤ 6). Nuclear and cytoplasmic expression of phospho-p53
251 (Ser20) was seen in all of 40 HSAs (100%), with 32 tumors (80%) showing high levels of
252 expression. These data revealed that patterns of p53 and activated p53 were comparable in
253 human ASs and canine HSAs; especially, p53 was strongly phosphorylated at residue Ser20 in

254 tumors from both species. We found no association between phosphorylated p53 and *TP53*
255 mutations or fusion genes (**fig. S10**), suggesting that DNA damage and cellular stress are
256 widespread among these tumors, and they are likely to activate p53-mediated repair mechanisms
257 independent of these genetic alterations.

258 The PI3K/AKT/mTOR signaling pathway is important for regulation of angiogenic,
259 vascular, and energetic functions. To assess whether PI3K mutations resulted in higher levels of
260 downstream pathway activation, we evaluated expression of AKT and phospho-AKT proteins in
261 human ASs and canine HSAs (**Fig. 5C-D**). Expression of nuclear and cytoplasmic AKT protein
262 was observed in all eleven human ASs (100%) with eight of eleven (73%) tumors showing
263 medium or high expression. Expression of phospho-AKT (Thr308) was evaluated in eight
264 tumors; all of them (100%) showed weak or medium levels of expression. Similarly, AKT
265 protein was detectable in the nucleus and cytoplasm of all forty (100%) canine HSAs with 37
266 (93%) showing medium or high expression. Phospho-AKT (Thr308) was detected in the nuclei
267 and cytoplasm of all evaluable 39 (100%) canine HSAs, with 34 (87%) expressing medium or
268 high level of the protein. Strong AKT immunoreactivity was also seen in scattered stromal cells
269 in both human AS and canine HSA. Neither mutations of *TP53*, *PIK3CA*, *PIK3R1* nor the
270 presence of fusion genes were associated with expression of AKT and phospho-AKT in human
271 or canine tumors (**fig. S11**). Since *PIK3CA* and *PIK3R1* mutations were undetectable in this set
272 of eleven human ASs, we examined expression of mTOR and phospho-mTOR (Ser2448)
273 proteins as surrogates to confirm activation of their downstream pathways in these tumors.
274 mTOR protein was observed in the nuclei and cytoplasm of all eleven tumors (IHC score ≥ 6),
275 and it was not associated with the presence of *TP53* mutations or fusions (**fig. S12A-B**).
276 However, nuclear and cytoplasmic expression of phospho-mTOR was higher in ASs that had

277 *TP53* mutations or that had fusion genes than it was in tumors without one of these genetic
278 changes (**Fig. S12C-D**).
279 In summary, the immunostaining data suggest that human AS and canine HSA have comparable
280 activation of the p53 and PI3K/AKT/mTOR pathways, and these events are largely independent
281 of their mutational states. Our results further suggest that these vasoformative tumors from both
282 species activate convergent signaling pathways that contribute to their final architecture and
283 organization with predictable enrichment of angiogenic gene signatures.
284

285 **Discussion**

286 For this study, our objective was to identify novel fusion genes in human ASs and spontaneous
287 canine HSAs. We showed that novel protein-coding fusion genes were identified in
288 approximately 50% of human ASs of which two had *TP53* mutations. In canine HSAs, protein-
289 coding fusion genes were detectable in ~15% of tumors, and those were associated with p53
290 deficiency and enrichment of angiogenic gene signatures. Our data suggest that convergent
291 molecular mechanisms associated with p53 inactivation and enhanced PI3K/AKT/mTOR
292 signaling pathways are operational in genomically complex human ASs and canine HSAs.
293

294 In the past decade, advances in next-generation sequencing and bioinformatics have
295 enabled genome-wide identification of unbiased cancer-associated fusion transcripts in a variety
296 of tumor types. Previous studies have reported 7,887 fusion transcripts identified across thirteen
297 tumor types in TCGA datasets and 9,928 fusion genes with a 3% recurrence rate in the Mitelman
298 Database of Chromosome Aberrations and Gene Fusions in Cancer (*29-31*). These findings
299 illustrate the complexity of the cancer-associated fusion gene landscape, showing a relatively

300 high rate of fusions with low recurrence, possibly arising from catastrophic chromosome
301 rearrangements by chromothripsis (*32*) and chromoplexy (*33*). Despite this relatively high
302 frequency of fusion genes, a solution to define their pathogenic significance remains elusive.
303 One key finding from this work was that protein-coding fusion genes co-occurred with mutations
304 of *TP53* in the angiogenic molecular subtype of canine HSA, suggesting that genomic instability
305 might create a predisposition for translocations and the resultant fusion genes and that, in turn,
306 these fusion genes create unique transcriptional programs that promote angiogenic phenotypes in
307 these p53-deficient backgrounds.
308
309 Specifically, kinase fusion genes involving *FLT1*, *PTK2*, and *AKT3* can activate key
310 convergent gene pathways associated with blood vessel formation and remodeling (*34*), and they
311 represent potential therapeutic targets for kinase inhibitors (*35, 36*). When we consider that
312 sarcomas have the highest frequency of kinase fusions in TCGA datasets (*35*), but that they also
313 have extremely low recurrence, a more rational approach might be to develop agents that target
314 these convergent angiogenic pathways instead of the products from the individual fusion genes
315 themselves (*37*).
316
317 The two fusion genes that we confirmed by genomic structural evaluation in canine
318 HSAs were present in approximately 20 - 40% of cells in the tumor, both genes showing chaotic
319 amplification. Several explanations could account for these observations. One is that histology
320 and bioinformatics assays overestimated tumor content and tumor purity. Another is that fusions
321 are epiphenomena arising from chaotic genomes with no influence on selection. A third, which
322 we believe is most likely, is that translocation and the resulting fusion events occur stochastically

323 in genomically unstable cells late in the course of tumor evolution. However, the enrichment of
324 fusion genes and angiogenic transcriptional programs suggests that these traits endow tumor cells
325 with selective growth and/or survival advantages that contribute to tumor progression by
326 promoting proangiogenic environments. It is worth noting that the selective pressures in the AS
327 milieu favor not only fusion-positive clones, but also fusion-negative clones, as the establishment
328 of a proangiogenic environment could improve survival of all the subpopulations within the
329 tumor. Indeed, a similar mechanism might be operative in alveolar rhabdomyosarcomas, where
330 *PAX3-FOXO1A* fusions are necessary for tumor initiation but have no effect on tumor recurrence
331 (*38, 39*). Further work will be necessary to distinguish which among these non-mutually
332 exclusive possibilities are operative, and to better understand the role of fusion genes in tumor
333 evolution of human AS and canine HSA and, potentially, in promoting clonal heterogeneity
334 through the creation of a permissive niche.
335
336 Fusion genes have been reported in human ASs (*10, 40-42*). For instance, one study
337 found a *CIC-LEUTX* fusion in one of 120 (0.8%) FFPE ASs examined (*10*); another found a
338 *CEP85L-ROS1* fusion in one of 34 (3.0%) ASs examined (*40*); and a third found an *EWSR1-*
339 *ATF1* fusion in one case of AS (*42*). A *NUP160-SLC43A3* fusion has also been reported in the
340 ISO-HAS AS cell line (*41*). However, none of these fusion genes has been identified recurrently
341 in subsequent studies of AS samples. While these observations are consistent with our stochastic
342 hypothesis, we cannot completely exclude the possibility that fusion genes in human ASs, or for
343 that matter in canine HSAs, are non-pathogenic passenger aberrations.
344

345 A larger case series will be required to define the fusion gene landscape in human AS,
346 but canine HSA provides potential insights for what might be expected. Mutations of *TP53* are
347 largely mutually exclusive of mutations in *KDR*, *PIK3CA*, and *RAS* gene family in human AS,
348 and the mutational patterns seem to be associated with the location of the primary tumor (*12, 17*).
349 We see a similar pattern emerge in a subset of canine HSA, and from our data we propose a
350 model that can be used as a foundation to test mechanistic links between the mutational and
351 transcriptional landscapes in malignant vascular tumors (**Fig. 4**) and determine their roles in
352 tumor progression. In this model, inflammatory HSAs harbor no mutations of *PIK3CA*, and only
353 rarely of *TP53*, maintaining sufficient genomic stability that disfavors formation of fusion genes.
354 Furthermore, the transcriptional programs in these inflammatory HSAs are weakly angiogenic,
355 and their permissive inflammatory environments restrain growth and metastasis. Conversely,
356 angiogenic HSAs harbor frequent mutations of *PIK3CA* and *TP53*, and fusion events. Mutations
357 of *PIK3CA* in p53-proficient backgrounds promote pro-angiogenic environments, while in p53-
358 deficient backgrounds, these mutations promote altered chromatin regulation and
359 immunomodulatory transcriptional programs. Finally, mutations of *TP53* enable genomic
360 instability with formation of fusion genes. These events are stochastic, but fusion genes that
361 promote pro-angiogenic transcriptional programs can enhance or even supplant the effects of
362 *PIK3CA* mutations and create environments that accelerate tumor growth and metastatic
363 propensity. Validation of this model could alter the paradigms for diagnosis and treatment of
364 human AS and canine HSA, as well as of other aggressive, genomically complex sarcomas that
365 affect humans and dogs alike.
366
367 **Materials and Methods**

368 **Dog tissue samples**

369 Seventy-six snap frozen and FFPE tissue samples were obtained from 74 dogs with HSAs.
370 Frozen and FFPE tissues samples from 10 dogs with splenic hematomas, which are benign
371 lesions with enlarged vascular spaces lined by endothelial cells, were used as controls. Samples
372 were obtained as part of medically necessary diagnostic procedures and were used for research
373 with owner consent. The origin of these samples was reported previously (*14, 21, 43-45*), or they
374 were collected from dogs with HSA or with splenic hematomas at the Veterinary Medical
375 Center, University of Minnesota. Procedures involving animal use were done with approval and
376 under the supervision of the University of Minnesota Animal Care and Use Committee
377 (protocols 1110A06186, 1507-32804A, 0802A27363, 1101A94713, 1312-31131A, and 1702-
378 34548A). The demographic characteristics of dogs ($N = 74$) from whom we acquired HSA and
379 non-malignant splenic hematomas ($N = 10$) are summarized in **table S1**.

380

381 **Human tissue samples**

382 Snap frozen and FFPE tissues for human biospecimens were obtained from the University of
383 Minnesota Biological Materials Procurement Network (UMN BioNet) and from the Cooperative
384 Human Tissue Network (CHTN) under their standardized patient consent protocols. The
385 demographic characteristics of human patients from whom we obtained ASs ($N = 13$) and normal
386 tissue samples ($N = 6$) are summarized in **table S2**.

387

388 **Histological assessment**

389 FFPE sections (4 μm) were stained with hematoxylin and eosin (H&E) and examined by
390 veterinary pathologists to assign a histological diagnosis of canine HSA. Solid, capillary,

391 cavernous, or mixed histological subtypes were assigned using accepted criteria (*46*); mitotic
392 index (MI) was calculated per 1,000 cells in 5-10 random fields under 400X magnification (*47*).
393 H&E slides were further reviewed for tumor content by two board-certified medical pathologists
394 (ML and PM) (*48*), with the percent of sample containing viable nucleated cells corresponding to
395 tumor recorded in a range of 0 to > 90% based on the planar surface of the sections. Diagnostic
396 and histopathology reports of human tissues were provided by the specimen providers, the UMN
397 BioNet and the CHTN.
398
399 **RNA isolation and generation of RNA-Seq libraries**
400 Total RNA was isolated from tissue samples using the TriPure Isolation Reagent (Roche Applied
401 Science, Indianapolis, IN, USA). The RNeasy Mini Kit (Qiagen, Valencia, CA, USA) was used
402 for clean-up according to the manufacturer's instructions. RNA-Seq from 74 canine HSA tissues
403 is published (*17, 21, 49, 50*) and available through the Gene Expression Omnibus
404 (http://www.ncbi.nlm. nih.gov/geo; accession number GSE95183) and the NCBI Sequence Read
405 Archive (accession number PRJNA562916). Also included was an additional data set generated
406 from two canine HSA tissues and from 10 non-malignant splenic hematoma tissues that had not
407 been published previously. Total RNA was also extracted from 13 human AS tissues and from
408 six normal tissues. Two µg of total RNA from each sample were quantified and assessed for
409 quality; RNA-Seq libraries were generated as described (*21*) using the TruSeq RNA sample
410 preparation kit (Illumina Inc., San Diego, CA). Sequencing was performed using HiSeq 2000 or
411 2500 systems (Illumina Inc.). Each sample was sequenced to a targeted depth of 20 – 80 million
412 paired-end reads with mate-pair distance of 50 bp. Primary analysis and demultiplexing were
413 performed using CASAVA software version 1.8.2 (Illumina Inc.) to verify the quality of the

414 sequence data. The end result of the CASAVA workflow was demultiplexed into FASTQ files
415 for analysis. Bioanalyzer quality control and RNA-Seq were performed at the University of
416 Minnesota Genomics Center (UMGC) or at the Broad Institute.
417
418 **Bioinformatics analysis**
419 The original FASTQ files generated from 76 canine HSAs and ten non-malignant splenic
420 hematomas were mapped to the dog reference genome (Canfam3.1). The FASTQ files prepared
421 from thirteen human ASs and six non-malignant tissues were mapped to the human reference
422 genome (GRCh38). Sequencing quality was assessed by FastQC. The deFuse algorithm (*51*)
423 was used to identify putative fusion events. To discriminate true fusion candidates from artifacts,
424 we included fusion events with exon boundaries in both fusion partners and excluded events
425 created from adjacent genes that showed breakpoint homology (>1). We also filtered highly
426 recurrent fusion events that were found at implausible frequencies across tumor and non-
427 malignant tissue samples (*35*) and transcription-induced chimeras. The split sequences of the
428 fusion genes were validated by *de novo* assembly using Trinity (*52*). TranscriptsToOrfs and
429 deFuse-Trinity tools verified the deFuse fusion predictions with Trinity-assembled transcripts
430 and open reading frames. TopHat2 was used to generate BAM files, and the Integrative
431 Genomics Viewer (IGV 2.3; Broad Institute, Cambridge, MA) was used to visualize the mate
432 pair sequences of fusion genes. A protein translation tool in Expert Protein Analysis System
433 (ExPASy; SIB Swiss Institute of Bioinformatics, Lausanne, Switzerland) was used to determine
434 in-frame fusion proteins. Tumor purity and microenvironment scores were assessed using the
435 bioinformatics tools ESTIMATE (*53*) and *xCell* (*28*).
436

437 **Reverse transcription polymerase chain reaction (RT-PCR) and Sanger sequencing**

438 RT-PCR was performed to validate fusion transcripts identified by deFuse (*54*). Briefly, cDNA
439 was synthesized using SuperScript® VILO cDNA Synthesis Kit and Master Mix (Invitrogen).
440 PCR amplification was performed using a conventional thermocycler with HotStarTaq DNA
441 polymerase (Qiagen) or using a LightCycler® 96 (Roche Applied Science, Indianapolis, IN,
442 USA) with FastStart SYBR Green Master Mix (Roche Applied Science). PCR primer pairs used
443 for fusion gene amplification are presented in the Results section. *GAPDH* was used as a control
444 for RNA integrity and for the RT-PCR reactions. The forward and reverse primer sequences for
445 *GAPDH* were 5'-GGA GTC CAC TGG CGT CTT CAC-3' and 5'-GAG GCA TTG CTG ATG
446 ATC TTG AGG-3', respectively. Relative mRNA values were expressed as delta-Ct values
447 normalized to *GAPDH*. Sanger sequencing was performed at the UMGC.

448

449 **FISH**

450 FISH was performed to detect *MYO16-PTK2* and *GABRA3-FLT1* fusion genes by designing
451 FISH probes derived from the genome-anchored canine CHORI-82 bacterial artificial
452 chromosome (BAC) library (*55*). Single locus probes were used for proximal *MYO16* at dog
453 chromosome (CFA) 22:57,565,917-57,750,789 (clone 183H20), distal *MYO16* at CFA
454 22:57,750,801-57,967,880 (clone 385H13), and *PTK2* at CFA 13:35,302,679-35,483,060 (clone
455 451H13) with distinct fluorescent tags. For *GABRA3-FLT1* fusion, break-apart FISH probes
456 were used for proximal *FLT1* at CFA 25:11,057,892-11,263,935 (clone 363B20) and distal *FLT1*
457 at CFA 25:11,274,078-11,471,538 (clone 235H9). The PureLink® HiPure Plasmid Maxiprep Kit
458 (Invitrogen) was used for BAC DNA extraction. For preparation and hybridization of FISH
459 probes, BAC DNA probes were labeled by Nick Translation Kit (Abbott Molecular) using

460 Green-500 dUTP, Orange-552 dUTP and Aqua-431 dUTP (Enzo Life Science). Labeled DNA
461 was precipitated in COT-1 DNA, salmon sperm DNA, sodium acetate and 95% ethanol, then
462 dried and resuspended in 50% formamide hybridization buffer. The Red-proximal *MYO16*,
463 Green-distal *MYO16* and Aqua-*PTK2* probes were combined into one 3-color FISH probe for
464 *MYO16-PTK2* fusion. The Red-proximal *FLT1* and Green-distal *FLT1* break-apart probes were
465 applied for the split *FLT1* gene.
466 FFPE sections (4 μm) were processed according to the Dako IQFISH protocol; probes
467 were applied to the slide and hybridized for 24 hours at 37°C in a humidified chamber. After
468 hybridization, slides were washed and counterstained with DAPI. Fluorescent signals were
469 visualized on an Olympus BX61 microscope workstation (Applied Spectral Imaging, Vista, CA)
470 with DAPI, FITC, Texas Red and Aqua filter sets. FISH images were captured using an
471 interferometer-based CCD cooled camera (ASI) and FISHView ASI software. A total of 200
472 interphase cells were examined for each sample. Non-malignant canine spleen tissues were used
473 as controls for the FISH experiment.
474
475 **Validation of somatic mutations using RNA-Seq data**
476 A pipeline was developed to identify the bases present at locations defined as somatic mutations
477 in the Tumor-Normal exome calls (*17*). Briefly, RNA-Seq data were mapped using the STAR-
478 Mapper (*56*) with STAR-FUSION mapping settings (*57*) to the Canfam3.1 or GRCh38 genome.
479 BAM files generated by STAR were sorted and indexed using Samtools (*58*). Starting from a file
480 containing somatic mutation locations and a file containing a list of BAM file locations, the
481 pipeline uses Samtools (*58*) functions to identify the bases present at each location at each file
482 and then reports whether a variant is found at that location. For inclusion within the variant file,

483 at least one sample must have at least 3 reads that support the variant and that represent greater
484 than 10% of all reads at that location.
485
486 **Gene expression profiling**
487 CLC Bio Genomics Workbench 10 (CLC Bio, Aarhus, Denmark) and DESeq2 R packages were
488 used to quantify gene expression and differential gene expression analysis as described (*59*).
489 Briefly, paired-end RNA-Seq data with mate-pair distance of 50 bp in FASTQ format were
490 imported, and sequencing quality was determined. Transcriptomics analysis was then performed
491 to generate the expression level of each gene presented as total reads by mapping the sequencing
492 reads to Canfam3.1 or GRCh38. Heatmaps and hierarchical clustering based on average linkage
493 were visualized using Cluster 3.0, Morpheus (https://clue.io/morpheus), or R packages. GO
494 Enrichment Analysis (*60-62*) or Ingenuity® Pathway Analysis software version 8.6 (Qiagen,
495 Redwood City, CA) were used to define biological functions, canonical pathways, and upstream
496 regulators associated with DEGs between groups using Benjamini-Hochberg multiple testing
497 corrections to evaluate significance. For gene expression profiling, unsupervised PCA and
498 hierarchical clustering were performed to define subtypes of canine HSAs as described
499 previously (*21*). Gene expression data of human sarcomas in TCGA database
500 (https://www.cancer.gov/tcga) were also compared with our data sets.
501
502 **TMA generation and IHC**
503 Canine TMA blocks were generated from 45 HSA tissues, including 32 tumors used for RNA-
504 Seq and eight non-tumor tissues (six splenic hematomas and two non-malignant liver samples).
505 Tissue cores of 1-mm diameter in quadruplicate from each sample were assembled in random

506 order in four TMA blocks. One TMA block with mouse tissues was generated for staining
507 controls. Immunostaining with CD31, Vimentin and Pan-Cytokeratin antibodies was evaluated to
508 support tumor content estimates. A human TMA block was generated from ten AS tissues and
509 six non-malignant tissues (submandibular gland, skin, breast adipose tissue, thigh skeletal
510 muscle, spleen, and lung).

511 Unstained TMA sections (4 μm) were de-paraffinized and rehydrated using standard
512 methods for IHC. All of the immunohistochemical assays, including validation for antibodies,
513 were performed and optimized at the UMN BioNet Histology Laboratory or the Veterinary
514 Diagnostic Laboratory at the University of Minnesota. Antibodies used for IHC are summarized
515 in **table S3**. The percentage of positive cells with immunostaining was scored from 0 to 3+,
516 where 0 reflects specific staining in <1% of the cells, 1+ reflects specific staining in <25% of the
517 cells, 2+ reflects specific staining in 25–75% of the cells, and 3+ reflects specific staining in
518 >75% of the cells. The intensity was assessed as weak, moderate, or strong. Immunostaining
519 results were scored by multiplying the percentage of positive cells by the intensity.

520

521 **Statistical analysis**

522 Chi-square or Fisher's exact test, was performed for contingency tables analysis. Continuous
523 values were analyzed by Welch's (Heteroscedastic) T-test or Mann-Whitney U test. Statistical
524 analysis was performed using GraphPad Prism 6 (GraphPad Software, Inc., San Diego, CA).
525 *P*-values are reported without inference of significance, consistent with the American Statistical
526 Association's Statement on Statistical Significance and P-Values (*63*).

527

528 **Supplementary Materials**

529 Fig. S1. Representative putative inter-chromosomal fusion transcripts in human AS and canine
530 HSA.
531 Fig. S2. Fusion genes and their association with tumor content and sequencing depth in canine
532 HSA tissues.
533 Fig. S3. Detection of representative fusion genes in canine HSA.
534 Fig. S4. Genetic alterations of fusion partner genes identified in human AS.
535 Fig. S5. Cell type enrichment analysis in human ASs and TCGA sarcomas.
536 Fig. S6. Three distinct molecular groups of canine HSAs.
537 Fig. S7. Kaplan-Meier probability of survival for dogs with angiogenic and inflammatory HSA.
538 Fig. S8. Association of the fusion events with demographic and histopathologic features in
539 canine HSA.
540 Fig. S9. Gene pathways associated with commonly enriched genes in tumors with fusion genes
541 and *TP53* mutations in canine HSA.
542 Fig. S10. Violin plots display IHC scores of p53, p-p53 (Ser15), and p-p53 (Ser20) in human AS
543 and canine HSA.
544 Fig. S11. Violin plots present IHC scores of AKT and p-AKT (Thr308) in human AS and canine
545 HSA.
546 Fig. S12. IHC scores of mTOR and p-mTOR (Ser2448) in human AS.
547 Table S1. Demographic and pathological features of dogs with HSA.
548 Table S2. Demographic and pathological features of human patients with AS.
549 Table S3. Primary antibodies for immunohistochemical evaluation.
550 Table S4. Gene ontology and biological functions of fusion partner genes in human ASs.
551 Table S5. Gene ontology and biological functions of fusion partner genes in canine HSAs.

552 Table S6. Detection of fusion genes in canine HSAs by RT-PCR.

553 Table S7. Biological functions associated with 490 upregulated genes in human ASs.

554 Table S8. Association of frequency between fusion genes, *TP53* and *PIK3CA* mutations.

555 Table S9. Association of fusion genes with dog signalment and tumor histology.

556 Table S10. Association of frequency between fusion genes, *TP53* and *PIK3CA* mutations.

557 Table S11. 41 differentially expressed genes in PF ($N = 4$) compared to P ($N = 9$) group.

558 Table S12. 212 differentially expressed genes in PF ($N = 4$) compared to PK ($N = 6$) group.

559 Table S13. 377 differentially expressed genes in PF ($N = 4$) compared to PFK ($N = 4$) group.

560 Table S14. Immunohistochemical features of human ASs.

561 Table S15. Immunohistochemical features of canine HSAs.

562

563 **References and Notes**

564 1. B. S. Taylor, J. Barretina, R. G. Maki, C. R. Antonescu, S. Singer, M. Ladanyi, Advances
565 in sarcoma genomics and new therapeutic targets. *Nat Rev Cancer* **11**, 541-557 (2011).

566 2. A. Neuville, D. Ranchere-Vince, A. P. Dei Tos, M. C. Montesco, I. Hostein, L. Toffolatti,
567 F. Chibon, D. Pissaloux, L. Alberti, A. V. Decouvelaere, S. Albert, C. R. Rossi, J. Y.
568 Blay, J. M. Coindre, Impact of molecular analysis on the final sarcoma diagnosis: a study
569 on 763 cases collected during a European epidemiological study. *Am J Surg Pathol* **37**,
570 1259-1268 (2013).

571 3. L. J. Helman, P. Meltzer, Mechanisms of sarcoma development. *Nat Rev Cancer* **3**, 685-
572 694 (2003).

573 4. A. Italiano, C. L. Chen, R. Thomas, M. Breen, F. Bonnet, N. Sevenet, M. Longy, R. G.
574 Maki, J. M. Coindre, C. R. Antonescu, Alterations of the p53 and PIK3CA/AKT/mTOR

575 pathways in angiosarcomas: a pattern distinct from other sarcomas with complex
576 genomics. *Cancer* **118**, 5878-5887 (2012).
577 5. D. Buehler, S. R. Rice, J. S. Moody, P. Rush, G. R. Hafez, S. Attia, B. J. Longley, K. R.
578 Kozak, Angiosarcoma outcomes and prognostic factors: a 25-year single institution
579 experience. *Am J Clin Oncol* **37**, 473-479 (2014).
580 6. G. Lahat, A. R. Dhuka, H. Hallevi, L. Xiao, C. Zou, K. D. Smith, T. L. Phung, R. E.
581 Pollock, R. Benjamin, K. K. Hunt, A. J. Lazar, D. Lev, Angiosarcoma: clinical and
582 molecular insights. *Ann Surg* **251**, 1098-1106 (2010).
583 7. J. Fayette, E. Martin, S. Piperno-Neumann, A. Le Cesne, C. Robert, S. Bonvalot, D.
584 Ranchere, P. Pouillart, J. M. Coindre, J. Y. Blay, Angiosarcomas, a heterogeneous group
585 of sarcomas with specific behavior depending on primary site: a retrospective study of
586 161 cases. *Ann Oncol* **18**, 2030-2036 (2007).
587 8. A. Smrke, J. Hamm, A. Karvat, C. Simmons, A. Srikanthan, A retrospective review of
588 145 patients with angiosarcoma: Radiation therapy, extent of resection and chemotherapy
589 are important predictors of survival. Molecular and Clinical Oncology. *Molecular and*
590 *Clinical Oncology* **13**, 179-185 (2020).
591 9. S. Behjati, P. S. Tarpey, H. Sheldon, I. Martincorena, P. Van Loo, G. Gundem, D. C.
592 Wedge, M. Ramakrishna, S. L. Cooke, N. Pillay, H. K. M. Vollan, E. Papaemmanuil, H.
593 Koss, T. D. Bunney, C. Hardy, O. R. Joseph, S. Martin, L. Mudie, A. Butler, J. W.
594 Teague, M. Patil, G. Steers, Y. Cao, C. Gumbs, D. Ingram, A. J. Lazar, L. Little, H.
595 Mahadeshwar, A. Protopopov, G. A. Al Sannaa, S. Seth, X. Song, J. Tang, J. Zhang, V.
596 Ravi, K. E. Torres, B. Khatri, D. Halai, I. Roxanis, D. Baumhoer, R. Tirabosco, M. F.
597 Amary, C. Boshoff, U. McDermott, M. Katan, M. R. Stratton, P. A. Futreal, A. M.

598 Flanagan, A. Harris, P. J. Campbell, Recurrent PTPRB and PLCG1 mutations in
599 angiosarcoma. *Nat Genet* **46**, 376-379 (2014).
600 10. S. C. Huang, L. Zhang, Y. S. Sung, C. L. Chen, Y. C. Kao, N. P. Agaram, S. Singer, W.
601 D. Tap, S. D'Angelo, C. R. Antonescu, Recurrent CIC Gene Abnormalities in
602 Angiosarcomas: A Molecular Study of 120 Cases With Concurrent Investigation of
603 PLCG1, KDR, MYC, and FLT4 Gene Alterations. *Am J Surg Pathol* **40**, 645-655 (2016).
604 11. C. R. Antonescu, A. Yoshida, T. Guo, N. E. Chang, L. Zhang, N. P. Agaram, L. X. Qin,
605 M. F. Brennan, S. Singer, R. G. Maki, KDR activating mutations in human
606 angiosarcomas are sensitive to specific kinase inhibitors. *Cancer Res* **69**, 7175-7179
607 (2009).
608 12. C. A. Painter, E. Jain, B. N. Tomson, M. Dunphy, R. E. Stoddard, B. S. Thomas, A. L.
609 Damon, S. Shah, D. Kim, J. Gomez Tejeda Zanudo, J. L. Hornick, Y. L. Chen, P.
610 Merriam, C. P. Raut, G. D. Demetri, B. A. Van Tine, E. S. Lander, T. R. Golub, N.
611 Wagle, The Angiosarcoma Project: enabling genomic and clinical discoveries in a rare
612 cancer through patient-partnered research. *Nat Med* **26**, 181-187 (2020).
613 13. C. Antonescu, Malignant vascular tumors--an update. *Mod Pathol* **27 Suppl 1**, S30-38
614 (2014).
615 14. A. R. Lamerato-Kozicki, K. M. Helm, C. M. Jubala, G. R. Cutter, J. F. Modiano, Canine
616 hemangiosarcoma originates from hematopoietic precursors with potential for endothelial
617 differentiation. *Exp Hematol* **34**, 870-878 (2006).
618 15. S. M. Cohen, R. D. Storer, K. A. Criswell, N. G. Doerrer, V. L. Dellarco, D. G. Pegg, Z.
619 W. Wojcinski, D. E. Malarkey, A. C. Jacobs, J. E. Klaunig, J. A. Swenberg, J. C. Cook,

620 Hemangiosarcoma in rodents: mode-of-action evaluation and human relevance. *Toxicol*
621 *Sci* **111**, 4-18 (2009).
622 16. C. Mullin, C. A. Clifford, Histiocytic Sarcoma and Hemangiosarcoma Update. *Vet Clin*
623 *North Am Small Anim Pract* **49**, 855-879 (2019).
624 17. K. Megquier, J. Turner-Maier, R. Swofford, J. H. Kim, A. L. Sarver, C. Wang, S.
625 Sakthikumar, J. Johnson, M. Koltookian, M. Lewellen, M. C. Scott, A. J. Schulte, L.
626 Borst, N. Tonomura, J. Alfoldi, C. Painter, R. Thomas, E. K. Karlsson, M. Breen, J. F.
627 Modiano, I. Elvers, K. Lindblad-Toh, Comparative Genomics Reveals Shared Mutational
628 Landscape in Canine Hemangiosarcoma and Human Angiosarcoma. *Mol Cancer Res* **17**,
629 2410-2421 (2019).
630 18. G. Wang, M. Wu, A. C. Durham, E. Radaelli, N. J. Mason, X. Xu, D. B. Roth, Molecular
631 subtypes in canine hemangiosarcoma reveal similarities with human angiosarcoma. *PLoS*
632 *One* **15**, e0229728 (2020).
633 19. R. Thomas, L. Borst, D. Rotroff, A. Motsinger-Reif, K. Lindblad-Toh, J. F. Modiano, M.
634 Breen, Genomic profiling reveals extensive heterogeneity in somatic DNA copy number
635 aberrations of canine hemangiosarcoma. *Chromosome Res* **22**, 305-319 (2014).
636 20. N. J. Andersen, B. J. Nickoloff, K. J. Dykema, E. A. Boguslawski, R. I. Krivochenitser,
637 R. E. Froman, M. J. Dawes, L. H. Baker, D. G. Thomas, D. A. Kamstock, B. E. Kitchell,
638 K. A. Furge, N. S. Duesbery, Pharmacologic inhibition of MEK signaling prevents
639 growth of canine hemangiosarcoma. *Mol Cancer Ther* **12**, 1701-1714 (2013).
640 21. B. H. Gorden, J. H. Kim, A. L. Sarver, A. M. Frantz, M. Breen, K. Lindblad-Toh, T. D.
641 O'Brien, L. C. Sharkey, J. F. Modiano, E. B. Dickerson, Identification of three molecular

642 and functional subtypes in canine hemangiosarcoma through gene expression profiling
643 and progenitor cell characterization. *Am J Pathol* **184**, 985-995 (2014).
644 22. J. H. Kim, A. M. Frantz, A. L. Sarver, B. H. Gorden Klukas, M. Lewellen, T. D. O'Brien,
645 E. B. Dickerson, J. F. Modiano, Modulation of fatty acid metabolism and immune
646 suppression are features of in vitro tumour sphere formation in ontogenetically distinct
647 dog cancers. *Vet Comp Oncol*, (2017).
648 23. R. Hill, Y. Song, R. D. Cardiff, T. Van Dyke, Selective evolution of stromal mesenchyme
649 with p53 loss in response to epithelial tumorigenesis. *Cell* **123**, 1001-1011 (2005).
650 24. I. Goldstein, V. Marcel, M. Olivier, M. Oren, V. Rotter, P. Hainaut, Understanding wild-
651 type and mutant p53 activities in human cancer: new landmarks on the way to targeted
652 therapies. *Cancer Gene Ther* **18**, 2-11 (2011).
653 25. F. Mitelman, B. Johansson, F. Mertens, The impact of translocations and gene fusions on
654 cancer causation. *Nat Rev Cancer* **7**, 233-245 (2007).
655 26. M. Breen, J. F. Modiano, Evolutionarily conserved cytogenetic changes in hematological
656 malignancies of dogs and humans--man and his best friend share more than
657 companionship. *Chromosome Res* **16**, 145-154 (2008).
658 27. K. Marley, C. S. Maier, S. C. Helfand, Phosphotyrosine enrichment identifies focal
659 adhesion kinase and other tyrosine kinases for targeting in canine hemangiosarcoma. *Vet*
660 *Comp Oncol* **10**, 214-222 (2012).
661 28. D. Aran, Z. Hu, A. J. Butte, xCell: digitally portraying the tissue cellular heterogeneity
662 landscape. *Genome Biol* **18**, 220 (2017).
663 29. F. Mertens, B. Johansson, T. Fioretos, F. Mitelman, The emerging complexity of gene
664 fusions in cancer. *Nat Rev Cancer* **15**, 371-381 (2015).

665 30. K. Yoshihara, Q. Wang, W. Torres-Garcia, S. Zheng, R. Vegesna, H. Kim, R. G.
666 Verhaak, The landscape and therapeutic relevance of cancer-associated transcript fusions.
667 *Oncogene* **34**, 4845-4854 (2015).
668 31. F. Mitelman, B. Johansson, F. Mertens, Mitelman Database Chromosome Aberrations
669 and Gene Fusions in Cancer. https://mitelmandatabase.isb-cgc.org/. (2020).
670 32. P. J. Stephens, C. D. Greenman, B. Fu, F. Yang, G. R. Bignell, L. J. Mudie, E. D.
671 Pleasance, K. W. Lau, D. Beare, L. A. Stebbings, S. McLaren, M. L. Lin, D. J. McBride,
672 I. Varela, S. Nik-Zainal, C. Leroy, M. Jia, A. Menzies, A. P. Butler, J. W. Teague, M. A.
673 Quail, J. Burton, H. Swerdlow, N. P. Carter, L. A. Morsberger, C. Iacobuzio-Donahue, G.
674 A. Follows, A. R. Green, A. M. Flanagan, M. R. Stratton, P. A. Futreal, P. J. Campbell,
675 Massive genomic rearrangement acquired in a single catastrophic event during cancer
676 development. *Cell* **144**, 27-40 (2011).
677 33. N. D. Anderson, R. de Borja, M. D. Young, F. Fuligni, A. Rosic, N. D. Roberts, S.
678 Hajjar, M. Layeghifard, A. Novokmet, P. E. Kowalski, M. Anaka, S. Davidson, M.
679 Zarrei, B. Id Said, L. C. Schreiner, R. Marchand, J. Sitter, N. Gokgoz, L. Brunga, G. T.
680 Graham, A. Fullam, N. Pillay, J. A. Toretsky, A. Yoshida, T. Shibata, M. Metzler, G. R.
681 Somers, S. W. Scherer, A. M. Flanagan, P. J. Campbell, J. D. Schiffman, M. Shago, L. B.
682 Alexandrov, J. S. Wunder, I. L. Andrulis, D. Malkin, S. Behjati, A. Shlien,
683 Rearrangement bursts generate canonical gene fusions in bone and soft tissue tumors.
684 *Science* **361**, (2018).
685 34. H. K. Lee, S. K. Chauhan, E. Kay, R. Dana, Flt-1 regulates vascular endothelial cell
686 migration via a protein tyrosine kinase-7-dependent pathway. *Blood* **117**, 5762-5771
687 (2011).

688 35. N. Stransky, E. Cerami, S. Schalm, J. L. Kim, C. Lengauer, The landscape of kinase
689 fusions in cancer. *Nat Commun* **5**, 4846 (2014).
690 36. P. Kim, P. Jia, Z. Zhao, Kinase impact assessment in the landscape of fusion genes that
691 retain kinase domains: a pan-cancer study. *Brief Bioinform* **19**, 450-460 (2018).
692 37. S. Medves, J. B. Demoulin, Tyrosine kinase gene fusions in cancer: translating
693 mechanisms into targeted therapies. *J Cell Mol Med* **16**, 237-248 (2012).
694 38. P. R. Pandey, B. Chatterjee, M. E. Olanich, J. Khan, M. M. Miettinen, S. M. Hewitt, F.
695 G. Barr, PAX3-FOXO1 is essential for tumour initiation and maintenance but not
696 recurrence in a human myoblast model of rhabdomyosarcoma. *J Pathol* **241**, 626-637
697 (2017).
698 39. J. L. Selfe, J. Shipley, Fusion gene addiction: can tumours be forced to give up the habit?
699 *J Pathol* **242**, 263-266 (2017).
700 40. C. P. Giacomini, S. Sun, S. Varma, A. H. Shain, M. M. Giacomini, J. Balagtas, R. T.
701 Sweeney, E. Lai, C. A. Del Vecchio, A. D. Forster, N. Clarke, K. D. Montgomery, S.
702 Zhu, A. J. Wong, M. van de Rijn, R. B. West, J. R. Pollack, Breakpoint analysis of
703 transcriptional and genomic profiles uncovers novel gene fusions spanning multiple
704 human cancer types. *PLoS Genet* **9**, e1003464 (2013).
705 41. N. Shimozono, M. Jinnin, M. Masuzawa, M. Masuzawa, Z. Wang, A. Hirano, Y.
706 Tomizawa, T. Etoh-Kira, I. Kajihara, M. Harada, S. Fukushima, H. Ihn, NUP160-
707 SLC43A3 is a novel recurrent fusion oncogene in angiosarcoma. *Cancer Res* **75**, 4458-
708 4465 (2015).

709 42. A. A. Gru, N. Becker, J. D. Pfeifer, Angiosarcoma of the parotid gland with a t(12;22)
710 translocation creating a EWSR1-ATF1 fusion: a diagnostic dilemma. *J Clin Pathol* **66**,
711 452-454 (2013).
712 43. S. P. Fosmire, E. B. Dickerson, A. M. Scott, S. R. Bianco, M. J. Pettengill, H.
713 Meylemans, M. Padilla, A. A. Frazer-Abel, N. Akhtar, D. M. Getzy, J. Wojcieszyn, M.
714 Breen, S. C. Helfand, J. F. Modiano, Canine malignant hemangiosarcoma as a model of
715 primitive angiogenic endothelium. *Lab Invest* **84**, 562-572 (2004).
716 44. E. B. Dickerson, R. Thomas, S. P. Fosmire, A. R. Lamerato-Kozicki, S. R. Bianco, J. W.
717 Wojcieszyn, M. Breen, S. C. Helfand, J. F. Modiano, Mutations of phosphatase and
718 tensin homolog deleted from chromosome 10 in canine hemangiosarcoma. *Vet Pathol* **42**,
719 618-632 (2005).
720 45. B. A. Tamburini, S. Trapp, T. L. Phang, J. T. Schappa, L. E. Hunter, J. F. Modiano, Gene
721 expression profiles of sporadic canine hemangiosarcoma are uniquely associated with
722 breed. *PLoS One* **4**, e5549 (2009).
723 46. J.-H. Kim, A. Graef, E. Dickerson, J. Modiano, Pathobiology of Hemangiosarcoma in
724 Dogs: Research Advances and Future Perspectives. *Veterinary Sciences* **2**, 388 (2015).
725 47. P. Rudolph, J. Peters, D. Lorenz, D. Schmidt, R. Parwaresch, Correlation between mitotic
726 and Ki-67 labeling indices in paraffin-embedded carcinoma specimens. *Hum Pathol* **29**,
727 1216-1222 (1998).
728 48. B. R. Tschida, N. A. Temiz, T. P. Kuka, L. A. Lee, J. D. Riordan, C. A. Tierrablanca, R.
729 Hullsiek, S. Wagner, W. A. Hudson, M. A. Linden, K. Amin, P. J. Beckmann, R. A.
730 Heuer, A. L. Sarver, J. D. Yang, L. R. Roberts, J. H. Nadeau, A. J. Dupuy, V. W. Keng,

731 D. A. Largaespada, Sleeping Beauty Insertional Mutagenesis in Mice Identifies Drivers
732 of Steatosis-Associated Hepatic Tumors. *Cancer Res* **77**, 6576-6588 (2017).
733 49. N. Tonomura, I. Elvers, R. Thomas, K. Megquier, J. Turner-Maier, C. Howald, A. L.
734 Sarver, R. Swofford, A. M. Frantz, D. Ito, E. Mauceli, M. Arendt, H. J. Noh, M.
735 Koltookian, T. Biagi, S. Fryc, C. Williams, A. C. Avery, J. H. Kim, L. Barber, K.
736 Burgess, E. S. Lander, E. K. Karlsson, C. Azuma, J. F. Modiano, M. Breen, K. Lindblad-
737 Toh, Genome-wide association study identifies shared risk loci common to two
738 malignancies in golden retrievers. *PLoS Genet* **11**, e1004922 (2015).
739 50. A. Borgatti, J. S. Koopmeiners, A. L. Sarver, A. L. Winter, K. Stuebner, D. Todhunter,
740 A. E. Rizzardi, J. C. Henriksen, S. Schmechel, C. L. Forster, J. H. Kim, J. Froelich, J.
741 Walz, M. S. Henson, M. Breen, K. Lindblad-Toh, F. Oh, K. Pilbeam, J. F. Modiano, D.
742 A. Vallera, Safe and Effective Sarcoma Therapy through Bispecific Targeting of EGFR
743 and uPAR. *Mol Cancer Ther* **16**, 956-965 (2017).
744 51. A. McPherson, F. Hormozdiari, A. Zayed, R. Giuliany, G. Ha, M. G. Sun, M. Griffith, A.
745 Heravi Moussavi, J. Senz, N. Melnyk, M. Pacheco, M. A. Marra, M. Hirst, T. O. Nielsen,
746 S. C. Sahinalp, D. Huntsman, S. P. Shah, deFuse: an algorithm for gene fusion discovery
747 in tumor RNA-Seq data. *PLoS Comput Biol* **7**, e1001138 (2011).
748 52. B. J. Haas, A. Papanicolaou, M. Yassour, M. Grabherr, P. D. Blood, J. Bowden, M. B.
749 Couger, D. Eccles, B. Li, M. Lieber, M. D. Macmanes, M. Ott, J. Orvis, N. Pochet, F.
750 Strozzi, N. Weeks, R. Westerman, T. William, C. N. Dewey, R. Henschel, R. D. Leduc,
751 N. Friedman, A. Regev, De novo transcript sequence reconstruction from RNA-seq using
752 the Trinity platform for reference generation and analysis. *Nat Protoc* **8**, 1494-1512
753 (2013).

754 53. K. Yoshihara, M. Shahmoradgoli, E. Martinez, R. Vegesna, H. Kim, W. Torres-Garcia,
755 V. Trevino, H. Shen, P. W. Laird, D. A. Levine, S. L. Carter, G. Getz, K. Stemke-Hale,
756 G. B. Mills, R. G. Verhaak, Inferring tumour purity and stromal and immune cell
757 admixture from expression data. *Nat Commun* **4**, 2612 (2013).
758 54. J. H. Kim, A. M. Frantz, K. L. Anderson, A. J. Graef, M. C. Scott, S. Robinson, L. C.
759 Sharkey, T. D. O'Brien, E. B. Dickerson, J. F. Modiano, Interleukin-8 promotes canine
760 hemangiosarcoma growth by regulating the tumor microenvironment. *Exp Cell Res* **323**,
761 155-164 (2014).
762 55. R. Thomas, S. E. Duke, E. K. Karlsson, A. Evans, P. Ellis, K. Lindblad-Toh, C. F.
763 Langford, M. Breen, A genome assembly-integrated dog 1 Mb BAC microarray: a
764 cytogenetic resource for canine cancer studies and comparative genomic analysis.
765 *Cytogenet Genome Res* **122**, 110-121 (2008).
766 56. A. Dobin, C. A. Davis, F. Schlesinger, J. Drenkow, C. Zaleski, S. Jha, P. Batut, M.
767 Chaisson, T. R. Gingeras, STAR: ultrafast universal RNA-seq aligner. *Bioinformatics* **29**,
768 15-21 (2013).
769 57. B. Haas, A. Dobin, N. Stransky, B. Li, X. Yang, T. Tickle, A. Bankapur, C. Ganote, T.
770 Doak, N. Pochet, J. Sun, C. Wu, T. Gingeras, A. Regev. (bioRxiv, 2017).
771 58. H. Li, B. Handsaker, A. Wysoker, T. Fennell, J. Ruan, N. Homer, G. Marth, G. Abecasis,
772 R. Durbin, S. Genome Project Data Processing, The Sequence Alignment/Map format
773 and SAMtools. *Bioinformatics* **25**, 2078-2079 (2009).
774 59. X. Qian, A. Khammanivong, J. M. Song, F. Teferi, P. Upadhyaya, E. Dickerson, F.
775 Kassie, RNA-sequencing studies identify genes differentially regulated during

776 inflammation-driven lung tumorigenesis and targeted by chemopreventive agents.
777 *Inflamm Res* **64**, 343-361 (2015).
778 60. M. Ashburner, C. A. Ball, J. A. Blake, D. Botstein, H. Butler, J. M. Cherry, A. P. Davis,
779 K. Dolinski, S. S. Dwight, J. T. Eppig, M. A. Harris, D. P. Hill, L. Issel-Tarver, A.
780 Kasarskis, S. Lewis, J. C. Matese, J. E. Richardson, M. Ringwald, G. M. Rubin, G.
781 Sherlock, Gene ontology: tool for the unification of biology. The Gene Ontology
782 Consortium. *Nat Genet* **25**, 25-29 (2000).
783 61. C. The Gene Ontology, The Gene Ontology Resource: 20 years and still GOing strong.
784 *Nucleic Acids Res* **47**, D330-D338 (2019).
785 62. H. Mi, A. Muruganujan, D. Ebert, X. Huang, P. D. Thomas, PANTHER version 14: more
786 genomes, a new PANTHER GO-slim and improvements in enrichment analysis tools.
787 *Nucleic Acids Res* **47**, D419-D426 (2019).
788 63. Ronald L. Wasserstein, N. A. Lazar, The ASA's Statement on p-Values: Context,
789 Process, and Purpose. *The American Statistician* **70**, 129-133 (2016).
790

791 **Acknowledgements**

792 The authors would like to acknowledge Dr. Corrie Painter for reviewing the manuscript and
793 providing feedback. The authors acknowledge Mitzi Lewellen for assistance with inventory,
794 database management, and editorial assistance. The authors would also like to thank Lauren
795 Mills for processing of the next generation sequencing data and Dr. Douglas Yee, Director of
796 Masonic Cancer Center, for assisting with the collection of human tissues. Human biospecimens
797 were obtained from the UMN BioNet and from the CHTN. This work was partially supported by
798 grants 1R03CA191713-01 (J.F. Modiano, A.L. Sarver, J.H. Kim) and R37CA218570 (E.K.

799 Karlsson) from the National Cancer Institute of the National Institutes of Health (NIH), grants
800 #422 (J.F. Modiano) and 1889-G (J.F. Modiano, M. Breen, K. Lindblad-Toh) from the AKC
801 Canine Health Foundation, grant JHK15MN-004 (J.H. Kim) from the National Canine Cancer
802 Foundation, grant D10-501 (J.F. Modiano, M. Breen, K. Lindblad-Toh) from Morris Animal
803 Foundation, and a grant from Swedish Cancerfonden (K. Lindblad-Toh). This work was also
804 supported by an NIH NCI R50 grant, CA211249 (A.L. Sarver). The NIH Comprehensive Cancer
805 Center Support Grant to the Masonic Cancer Center, University of Minnesota (P30 CA077598)
806 provided support for the cytogenetic analyses performed in the Cytogenomics Shared Resource.
807 K. Megquier is supported by the National Cancer Institute of the NIH under Award Number
808 F32CA247088. The content is solely the responsibility of the authors and does not necessarily
809 represent the official views of the NIH. M. Breen is supported in part by the Oscar J. Fletcher
810 Distinguished Professorship in Comparative Oncology Genetics at North Carolina State
811 University. K. Lindblad-Toh is supported by a Distinguished Professor award from the Swedish
812 Research Council. J.F. Modiano is supported by the Alvin and June Perlman Chair in Animal
813 Oncology. The results shown in this study include RNA-Seq gene expression data generated by
814 the TCGA Research Network (https://www.cancer.gov/tcga) as well as data from The
815 Angiosarcoma Project (https:// ascproject.org/), a project of Count Me In
816 (https://joincountmein.org/). The UMGC (http://genomics.umn.edu) supported for generation of
817 genomic sequencing data libraries, and the Minnesota Supercomputing Institute (MSI) at the
818 University of Minnesota (http://www.msi.umn.edu) provided computational resources that
819 contributed to the results in this study. The authors gratefully acknowledge donations to the
820 Animal Cancer Care and Research Program of the University of Minnesota that helped support
821 this project.

822

823 **Figures**

824 **Fig. 1.** Identification of novel putative protein-coding fusion transcripts in human AS and canine

825 HSA

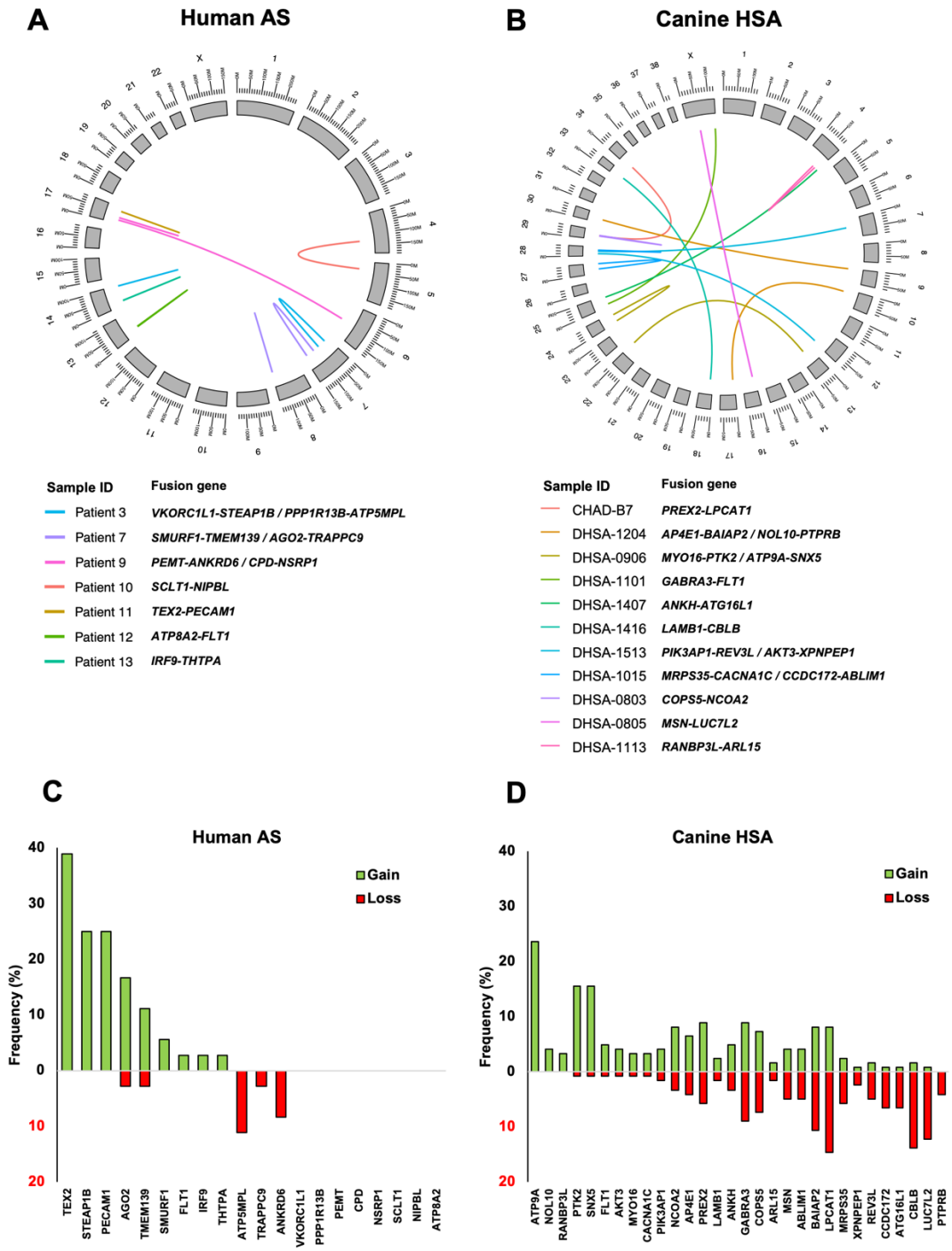

826

827 **Fig. 1.** Identification of novel putative protein-coding fusion transcripts in human AS and canine
828 HSA. The *Circos* plots visualize fusion genes identified in human ASs (**A**, $N = 13$) and canine
829 HSA (**B**, $N = 76$). Bar graphs show DNA copy number alterations for each fusion partner gene
830 using publicly available Exome-sequencing data in an independent dataset of human AS (**C**, $N =$
831 36; data retrieved from Ref [*12*]) and using oaCGH in a larger HSA dataset (**D**, $N = 123$; data
832 retrieved from Ref [*19*]).

833 **Fig. 2.** Validation of fusion genes in canine HSA

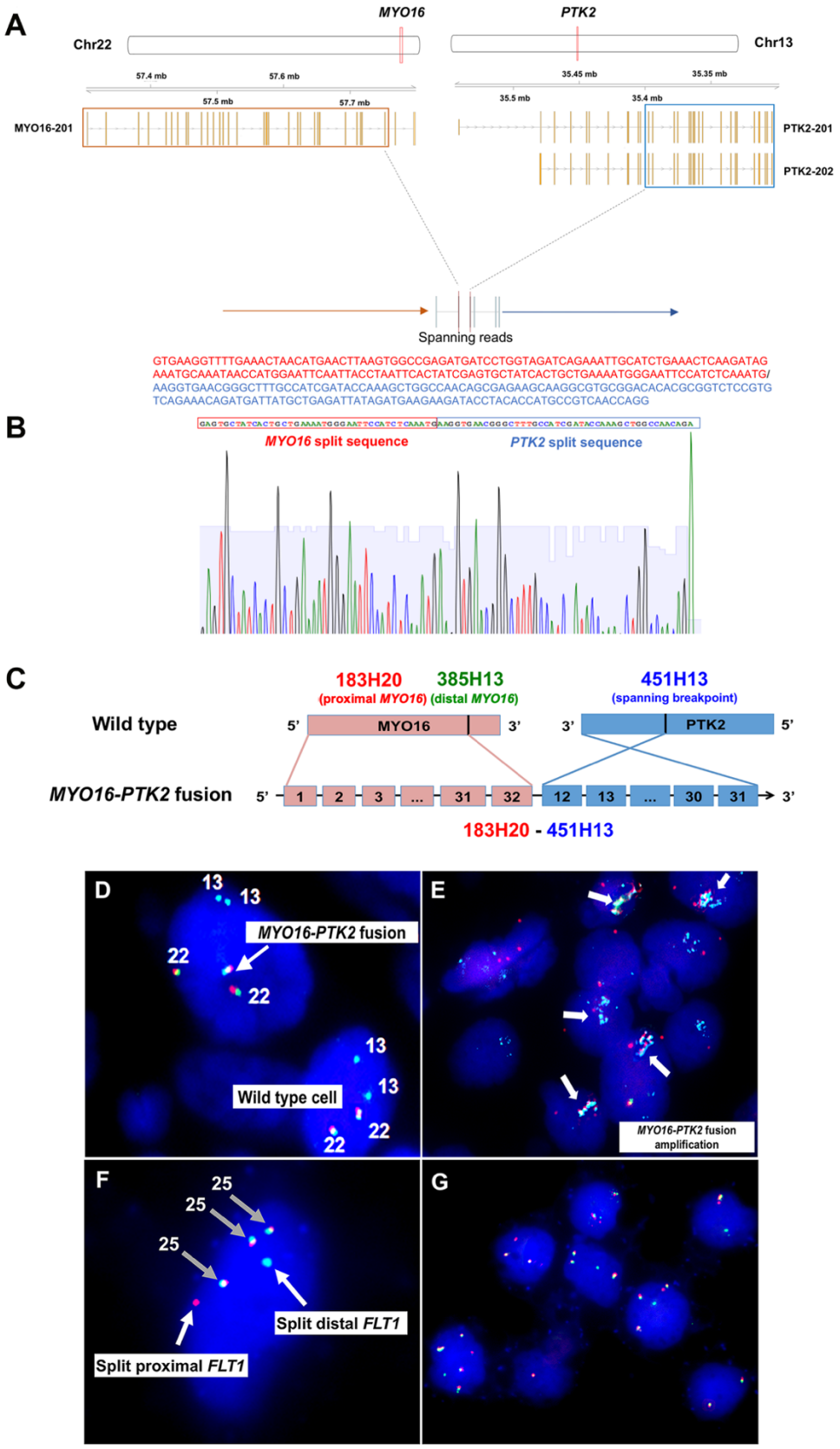

834

835 **Fig. 2.** Validation of fusion genes in canine HSA. **A,** *MYO16-PTK2* fusion gene track and
836 visualization of the breakpoint in UCSC Genome Browser (Canfam3.1). **B,** Sanger sequencing
837 result of the PCR product for *MYO16-PTK2* fusion gene. **C,** Schematic illustration of the
838 putative *MYO16-PTK2* fusion gene and designed FISH probes. **D,** Detection of the *MYO16-*
839 *PTK2* fusion gene on primary canine HSA tissue by FISH. In wild type cells an association
840 between BAC clones 183H20 (red) and 385H13 (green) can be appreciated, both showing
841 independent localization from 451H13 (aqua). A portion of tumor cells shows a breakage
842 within 451H13, with one half of that signal associating with 183H20, and independent of the
843 localization of 385H13 indicating the existence of the *MYO16-PTK2* fusion at the genomic level.
844 **E,** Arrows indicate the amplification of the *MYO16-PTK2* fusion gene. **F,** Detection of the
845 *GABRA3-FLT1* fusion gene by FISH. The *GABRA3-FLT1* fusion is identified by break-apart
846 FISH probes for proximal *FLT1* (clone 363B20; red) at CFA 25 and distal *FLT1* at CFA 25
847 (clone 235H9; green). Split *FLT1* genes indicate the fusion event identified by single color signal
848 (white arrows). Dual colors represent the intact *FLT1* gene (grey arrows). **G,** DNA amplification
849 of *FLT1* gene.

850 **Fig. 3**. Fusion genes, mutations of somatic variants, and molecular subtypes of human AS and

851 canine HSA

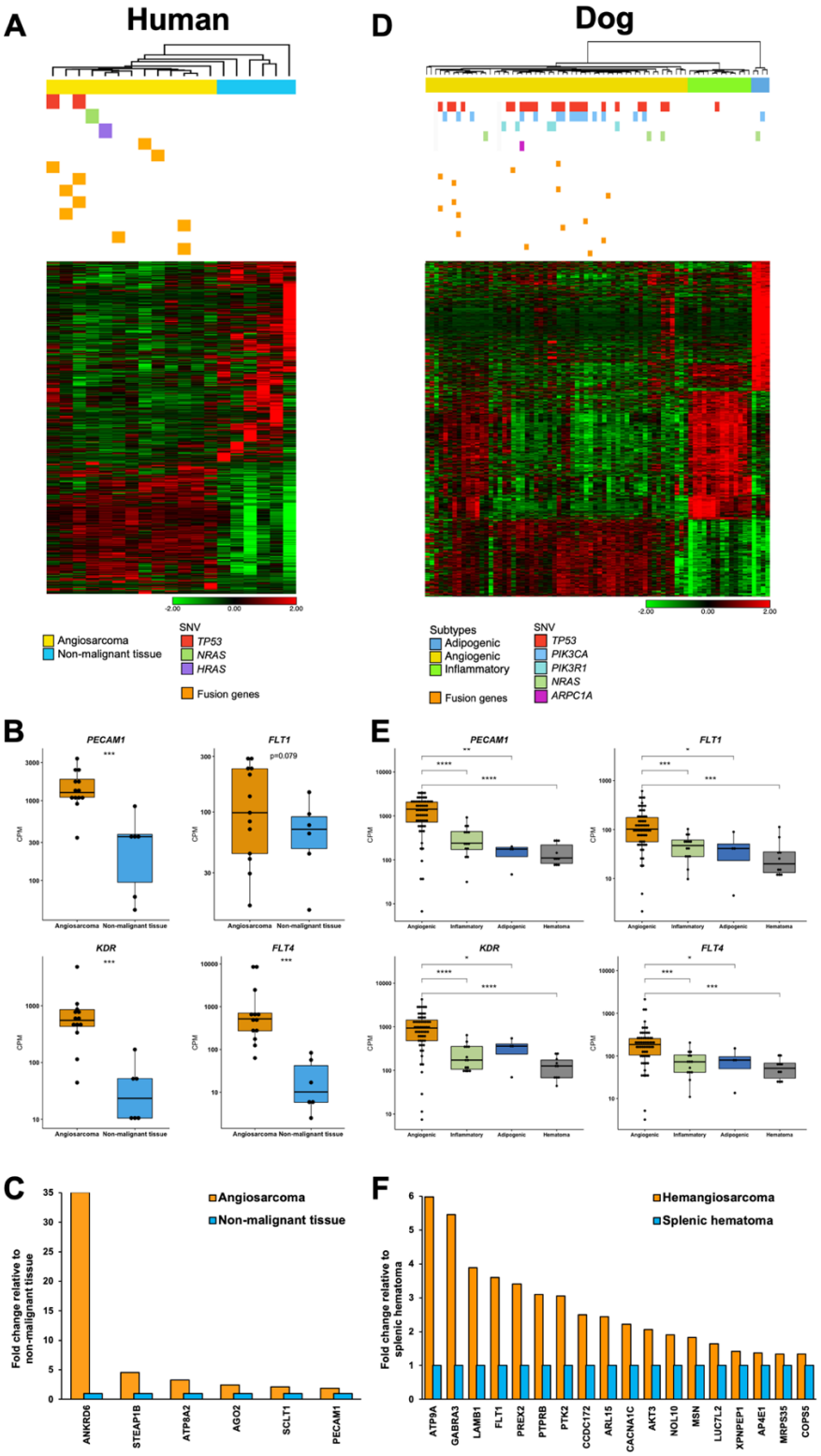

852

853 **Fig. 3.** Fusion genes, mutations of somatic variants, and molecular subtypes of human AS (A-C)
854 and canine HSA (D-F). **A,** 1,237 differentially expressed genes were identified between human
855 ASs ($N = 13$) and non-malignant tissue samples ($N = 6$) (False Discovery Rate or FDR $P < 0.05$):
856 490 genes were upregulated and 747 genes were downregulated in ASs. Ten fusion genes are
857 marked as yellow bars in seven AS samples. Somatic variations in *TP53* ($N = 2$), *NRAS* ($N = 1$),
858 and *HRAS* ($N = 1$) were found in four ASs. **B,** Box plots show gene expression of *PECAM1,*
859 *FLT1*, *KDR*, and *FLT4* representing vasculogenic and angiogenic functions in human ASs and
860 non-malignant tissues (Mann-Whitney test). ***, $P < 0.001$. **C**, Bar graphs show the relative
861 expression of genes in human ASs normalized to the expression of non-malignant tissues. Six of
862 20 genes where the *P*-value was less than 0.05 are displayed (Welch's T-test). **D,** Heatmap
863 illustrates 1,477 significant differentially expressed genes among three subtypes of canine HSA
864 ($N = 76$) (FDR $P < 0.001$; Fold change > 3). Somatic variant analysis identified mutations in
865 *TP53* ($N = 24$), *PIK3CA* ($N = 16$), *PIK3R1* ($N = 5$), *NRAS* ($N = 4$), and *ARPC1A* ($N = 1$). Grey
866 bars indicate unavailable somatic variants data. Fifteen fusion genes are marked as yellow bars in
867 11 HSA samples. **E,** Box plots display gene expression of *PECAM1, FLT1*, *KDR*, and *FLT4*
868 representing vasculogenic and angiogenic functions in subtypes of HSA and non-malignant
869 hematomas (Mann-Whitney test). ****, $P < 0.0001$; ***, $P < 0.001$; **, $P < 0.01$; *, $P < 0.05$. **F**,
870 Bar graphs show the relative expression of genes in canine HSA normalized to the expression of
871 hematomas. Eighteen of 30 genes where the P-value is less than 0.05 are displayed (Welch's T-
872 test). Heatmaps (**A** and **D**) show unsupervised hierarchical clustering (average linkage). Heatmap
873 colors display mean-centered fold change expression following $\log_2$ transformation. Upregulated
874 genes are presented in red and downregulated genes are shown in green.
875

876 **Fig. 4.** Hypothetical model for angiogenic pathogenesis of canine HSA

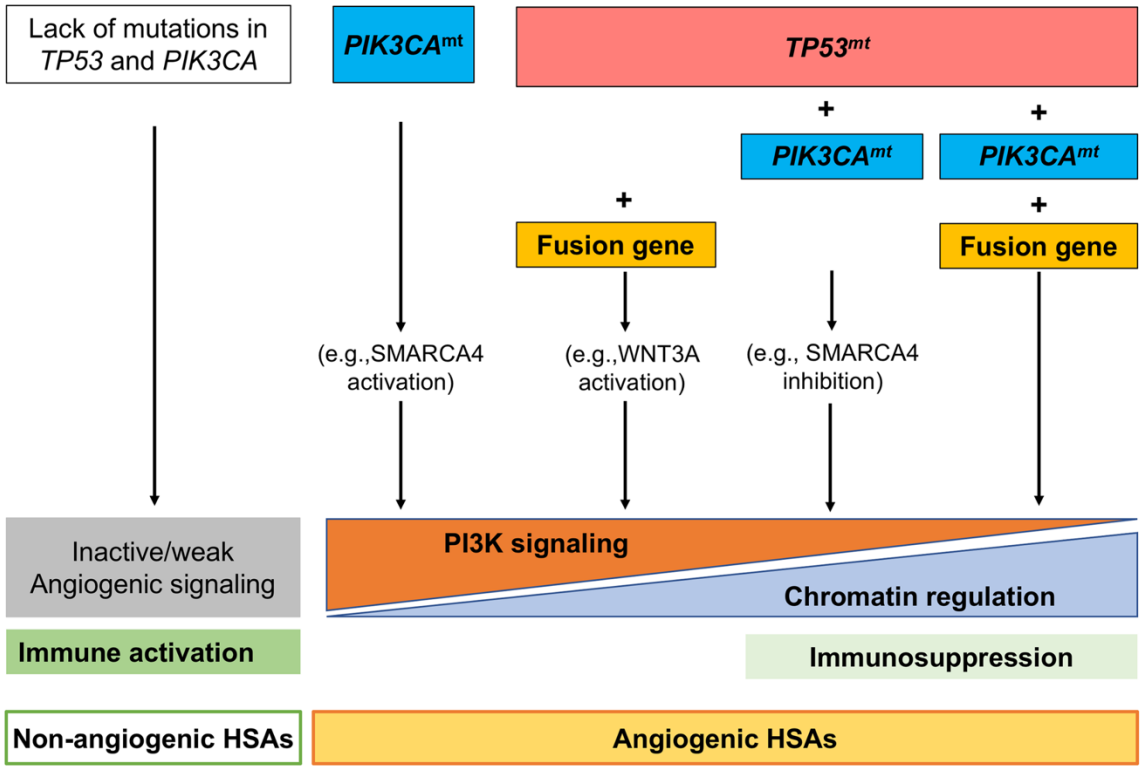

877

878

879 **Fig. 5.** Immunohistochemical expression of p53 and AKT proteins in human AS and canine

880 HSA.

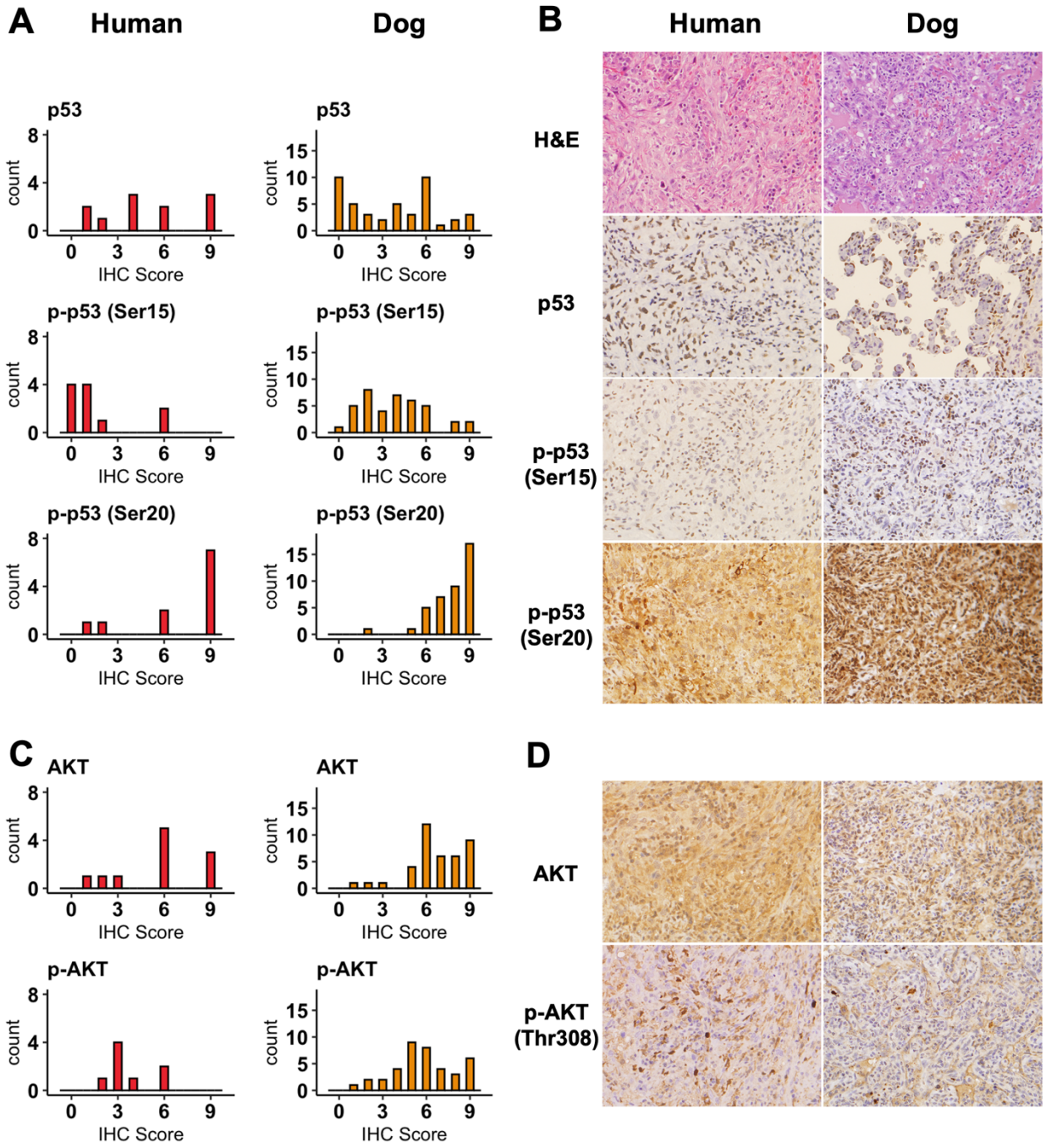

881

882

883 **Fig. 5.** Immunohistochemical expression of p53 and AKT proteins in human AS and canine
884 HSA. **A,** Bar graphs show the number of cases (y-axis) plotted as a function of IHC scores (x-
885 axis) for staining with anti-p53, anti-phosphorylated (p)-p53 (Ser15), and anti-p-p53 (Ser20)
886 antibodies in human ASs (Left panel) and canine HSAs (Right panel). **B,** Representative
887 photomicrographs show IHC staining of p53, p-p53 (Ser15), and p-p53 (Ser20) in human AS
888 (Left panel) and canine HSA tissues (Right panel). Bar graphs (**C**) for IHC scores of AKT and p-
889 AKT (Thr308) proteins and representative photomicrographs (**D**) are also displayed for human
890 ASs and canine HSAs. H&E = hematoxylin and eosin stain. IHC staining (Horseradish
891 peroxidase and hematoxylin counterstain). 200X magnification.
892
893 **Tables**
894 **Table 1.** Putative fusion genes identified in transcriptomic data of human ASs.
895 **Table 2.** Putative fusion genes identified in transcriptomic data of canine HSAs.

Table 1. Putative fusion genes identified in transcriptomic data of human ASs

Patient ID	Gene 1	Gene 2	Putative fusion gene	Gene 1 chromosome	Gene 2 chromosome	Gene 1 fusion location	Gene 2 fusion location	Fusion Type	Gene 1 Ensembl ID	Gene 2 Ensembl ID	Genomic break position in gene 1	Genomic break position in gene 2	Somatic variants
Patient 1	-	-	-	-	-	-	-	-	-	-	-	-	-
Patient 2	-	-	-	-	-	-	-	-	-	-	-	-	-
Patient 3	*VKORC1L1*	*STEAP1B*	*VKORC1L1-STEAP1B*	7	7	coding	coding	Intra-chromosomal	ENSG00000196715	ENSG00000105889	65873565	22419836	-
	PPP1R13B	*ATP5MPL*	*PPP1R13B-ATP5MPL*	14	14	coding	coding	Intra-chromosomal	ENSG00000088808	ENSG00000156411	103847299	103915189	
Patient 4	-	-	-	-	-	-	-	-	-	-	-	-	-
Patient 5	-	-	-	-	-	-	-	-	-	-	-	-	*HRAS*
Patient 6	-	-	-	-	-	-	-	-	-	-	-	-	-
Patient 7	*SMURF1*	*TMEM139*	*SMURF1-TMEM139*	*7*	*7*	coding	intron	Intra-chromosomal	ENSG00000198742	ENSG00000178826	99143726	143286424	*TP53*
	AGO2	*TRAPPC9*	*AGO2-TRAPPC9*	*8*	*8*	coding	coding	Intra-chromosomal	ENSG00000123908	ENSG00000167632	140635485	140451383	
Patient 8	-	-	-	-	-	-	-	-	-	-	-	-	*NRAS*
Patient 9	*PEMT*	*ANKRD6*	*PEMT-ANKRD6*	17	6	coding	utr5p	Inter-chromosomal	ENSG00000133027	ENSG00000135299	17577027	89433375	-
	CPD	*NSRP1*	*CPD-NSRP1*	17	17	coding	coding	Intra-chromosomal	ENSG00000108582	ENSG00000126653	30461311	30172542	
Patient 10	*SCLT1*	*NIPBL*	*SCLT1-NIPBL*	4	5	coding	coding	Inter-chromosomal	ENSG00000151466	ENSG00000164190	128888679	37057186	-
Patient 11	*TEX2*	*PECAM1*	*TEX2-PECAM1*	17	17	utr5p	utr5p	Intra-chromosomal	ENSG00000136478	ENSG00000261371	64263168	64390763	-
Patient 12	*ATP8A2*	*FLT1*	*ATP8A2-FLT1*	13	13	coding	coding	Intra-chromosomal	ENSG00000132932	ENSG00000102755	25968679	28357685	-
Patient 13	*IRF9*	*THTPA*	*IRF9-THTPA*	14	14	coding	coding	Intra-chromosomal	ENSG00000213928	ENSG00000259431	24164134	23558695	*TP53*

Table 2. Putative fusion genes identified in transcriptomic data of canine HSAs

Dog sample ID	Gene 1	Gene 2	Putative fusion gene	Gene 1 chromosome	Gene 2 chromosome	Gene 1 fusion location	Gene 2 fusion location	Fusion type	Gene 1 Ensembl ID	Gene 2 Ensembl ID	Genomic break position in gene 1	Genomic break position in gene 2	Somatic variants	
CHAD-B7	PREX2	LPCAT1	*PREX2-LPCAT1*	29	34	coding	coding	Inter-chromosomal	ENSCAFG00000007620	ENSCAFG00000010491	17653781	11166324	*TP53*	-
DHSA-1204	AP4E1	BAIAP2	*AP4E1-BAIAP2*	30	9	coding	coding	Inter-chromosomal	ENSCAFG00000015318	ENSCAFG00000005700	16748493	968509	*TP53*	-
	NOL10	PTPRB	*NOL10-PTPRB*	17	10	coding	coding	Inter-chromosomal	ENSCAFG00000003435	ENSCAFG00000000446	7515966	12372230		
DHSA-0906	MYO16	PTK2	*MYO16-PTK2*	22	13	coding	coding	Inter-chromosomal	ENSCAFG00000006050	ENSCAFG00000001217	57750807	35397284	*TP53*	-
	ATP9A	SNX5	*ATP9A-SNX5*	24	24	coding	coding	Intra-chromosomal	ENSCAFG00000011659	ENSCAFG00000005463	37856900	5096627		
DHSA1101	GABRA3	FLT1	*GABRA3-FLT1*	X	25	utr5p	coding	Inter-chromosomal	ENSCAFG00000019161	ENSCAFG00000006701	120379631	11232377	*TP53*	-
DHSA1407	ANKH	ATG16L1	*ANKH-ATG16L1*	4	25	coding	coding	Inter-chromosomal	ENSCAFG00000014290	ENSCAFG00000011752	88259666	44761299	-	-
DHSA1416	LAMB1	CBLB	*LAMB1-CBLB*	18	33	coding	coding	Inter-chromosomal	ENSCAFG00000025057	ENSCAFG00000009793	12675054	11259031	*TP53*	*PIK3CA*
DHSA1513	PIK3AP1	REV3L	*PIK3AP1-REV3L*	28	12	coding	coding	Inter-chromosomal	ENSCAFG00000008880	ENSCAFG00000003942	10085967	67953124	*TP53*	*PIK3CA*
	AKT3	XPNPEP1	*AKT3-XPNPEP1*	7	28	coding	coding	Inter-chromosomal	ENSCAFG00000015806	ENSCAFG00000010661	34778111	21321899		
DHSA-1015	MRPS35	CACNA1C	*MRPS35-CACNA1C*	27	27	coding	coding	Intra-chromosomal	ENSCAFG00000010963	ENSCAFG00000016051	20003244	44487698	-	*PIK3CA*
	CCDC172	ABLIM1	*CCDC172-ABLIM1*	28	28	coding	coding	Intra-chromosomal	ENSCAFG00000011803	ENSCAFG00000011513	26980198	25377079		
DHSA-0803	COPS5	NCOA2	*COPS5-NCOA2*	29	29	utr5p	utr5p	Intra-chromosomal	ENSCAFG00000007386	ENSCAFG00000007775	16578975	19448341	*TP53*	*PIK3CA*
DHSA-0805	MSN	LUC7L2	*MSN-LUC7L2*	X	16	coding	coding	Inter-chromosomal	ENSCAFG00000016607	ENSCAFG00000004069	50748329	9413652	*TP53*	*PIK3CA*
DHSA-1113	RANBP3L	ARL15	*RANBP3L-ARL15*	4	4	coding	coding	Intra-chromosomal	ENSCAFG00000018711	ENSCAFG00000018394	72325076	61484049	-	-